

Inference with generalizable classifier predictions

Ciaran Evans^{*1}, Zara Y. Weinberg², Manojkumar A. Puthenveedu³, and Max G'Sell¹

¹Department of Statistics and Data Science, Carnegie Mellon University

²Department of Biochemistry and Biophysics, University of California, San Francisco

³Department of Pharmacology, University of Michigan

Abstract

This paper addresses the problem of making statistical inference about a population that can only be identified through classifier predictions. The problem is motivated by scientific studies in which human labels of a population are replaced by a classifier. For downstream analysis of the population based on classifier predictions to be sound, the predictions must generalize equally across experimental conditions. In this paper, we formalize the task of statistical inference using classifier predictions, and propose bootstrap procedures to allow inference with a generalizable classifier. We demonstrate the performance of our methods through extensive simulations and a case study with live cell imaging data.

1 Introduction

This paper studies statistical issues that arise when classifiers are used to automate labor-intensive data collection in scientific pipelines. With data collection often requiring laborious human labels of objects or events, it has become common to apply automated labeling techniques, in which a classifier is trained on labeled examples to predict labels in new data (Norouzzadeh et al., 2018; Christiansen et al., 2018; Caicedo et al., 2019). These classifier predictions, rather than ground truth labels, are then used for statistical inference across groups and experimental conditions.

However, unless the classifier is perfect in all experimental settings, any inference based on the classifier predictions must incorporate the additional variability introduced by the classifier. Furthermore, to make valid comparisons across experimental units or conditions, the classifier must exhibit the same performance across those units and conditions. Since the purpose of the study is often to show that two conditions are actually different, this requirement is often unsatisfied unless explicitly designed for.

Motivated by experiments in which classifier predictions are the only feasible way to label large quantities of data, we present methodology for carrying out inference based on classifier-labeled data. We focus in particular on accounting for differences in data distribution between conditions. We outline considerations in designing a classifier beyond simple accuracy, and define the necessary assumptions and models to perform valid statistical inference. Our work is inspired by the following case study from cellular biology.

Motivating example: Studying cellular transport through exocytosis. Receptors on the cell surface play a crucial role in a cell's response to external stimuli. These receptors—and thus the corresponding responsiveness—are regulated in part by a process called *exocytosis*, which brings new receptors to the surface by packaging them on bubbles of membrane, which then merge with the outer membrane of the cell (Figure 1) (Yu et al., 1993; Pippig et al., 1995). Biologists can observe and measure exocytosis using *total*

*clevans@andrew.cmu.edu

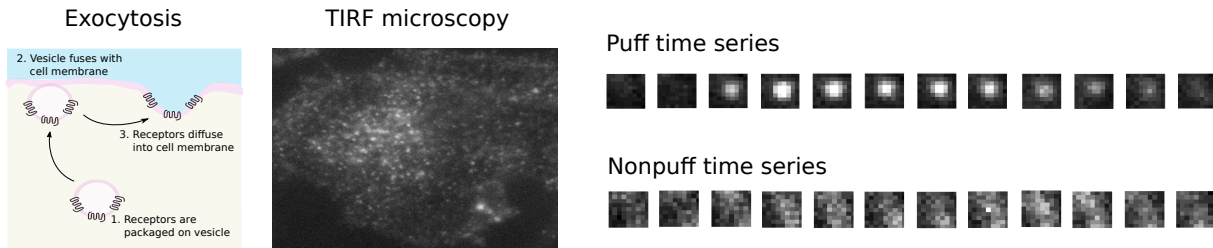


Figure 1: Fluorescent proteins are used to study exocytosis with TIRF microscopy. Left: Exocytosis regulated the concentration of receptor proteins on the cell surface by adding receptors through vesicle fusion. Center: The surface of a cell in a TIRF microscopy image; bright spots correspond to concentrated clusters of receptors on the cell surface. Right: Consecutive frames showing behavior of an exocytic event over time, in a 50Hz microscopy video. True exocytic events (“puffs”) have a characteristic pattern of diffusion over time. Other bright spots on the cell surface are not puffs, and do not show puff behavior.

internal reflection fluorescence (TIRF) microscopy, in which individual exocytotic events manifest as bright “puffs” of fluorescence on the cell surface, as fluorescence-tagged receptors are deposited and then diffuse (Figure 1) (Axelrod, 1981; Sankaranarayanan et al., 2000; Rappoport et al., 2003). For simplicity, we’ll refer to exocytic events as *puffs* for this reason. However, measuring these events is complicated by the fact that other objects and processes in the cell can also manifest as bright spots in these TIRF videos. Indeed, each cell in the data discussed in this paper typically has 5000 - 10000 detected events, and only about 5% are puffs.

A typical experiment compares puff behavior for several different surface receptors or experimental conditions, resulting in a hierarchical structure common to biological experiments, shown in Figure 2. When TIRF microscopy images are labeled by hand, statistical inference between conditions is straightforward:

1. TIRF microscopy is performed for each cell
2. Researchers use characteristic patterns of puff appearance to identify puffs (Logan et al., 2017; Kou et al., 2019)
3. Features describing puff behavior (e.g., how long diffusion takes, what diffusion looks like, etc.) are recorded (Yudowski et al., 2006; Bowman et al., 2015; Bohannon et al., 2017)
4. These features are compared across conditions

However, the volume of detected events in each cell makes manual labeling challenging. Automated labeling is therefore valuable, using a classifier trained to predict whether a bright spot is a puff or nonpuff. These predictions are then used for inference in place of hand labels.

Problem statement. Inspired by this motivating example, we consider data with the following structure, notated $\{(V_i, Y_i, C_i, K_i)\}_{i=1}^n$, where $Y \in \mathcal{Y}$ is the *unobserved* true label, V is a set of observed covariates, $C \in \mathcal{C}$ is experimental condition, and $K \in \mathcal{K}$ is a grouping variable nested within C that captures the hierarchical structure of the data. For instance, in the TIRF microscopy example, $Y \in \{0, 1\}$ denotes whether each event is a puff, V is a set of features derived from the microscopy images (either specially designed, or created by methods like convolutional neural networks), C denotes condition/receptor type, and K denotes the cell (Figure 2). More generally, C may indicate an experimental condition, and K a repetition of that experiment. We present the problem in this hierarchical setting because it is most common, and note that our methods can be simplified when the hierarchical structure does not apply.

Comparing experimental conditions $C \in \mathcal{C}$ often involves asking one or both of the following questions:

1. How does label prevalence $P(Y = y|C = c)$ vary for conditions $c \in \mathcal{C}$?

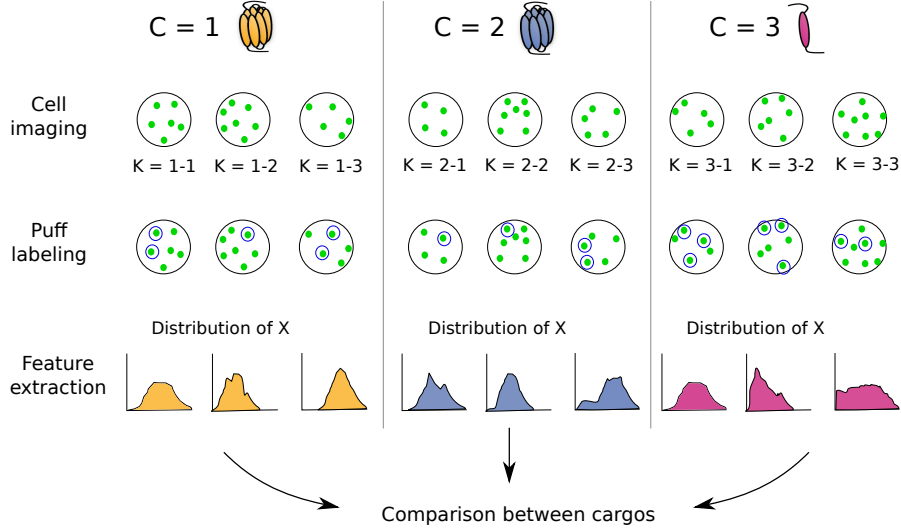


Figure 2: Overview of an experiment to compare exocytic events between three different conditions ($C = 1, 2, 3$). For each condition, several cells K are imaged with TIRF microscopy, and bright spots are identified. These detected events are then labeled as puffs or nonpuffs, and a feature X is recorded for each puff. The distribution of X is then compared across conditions.

2. How does the conditional distribution of $X|Y = y, C = c$ vary for conditions $c \in \mathcal{C}$, where $X \in \mathbb{R}$, $X \subset V$, denotes a feature of interest?

Crucially, Y is unobserved in new experimental data. To perform inference with unlabeled data, we have access to *labeled* training data $\{(V'_j, Y'_j, C'_j, K'_j)\}_{j=1}^m$, with the same set of labels $Y'_j \in \mathcal{Y}$, but different conditions $C'_j \in \mathcal{C}'$ and $K'_j \in \mathcal{K}'$. As new studies and experiments typically investigate different conditions, training and test data necessarily come from different experimental conditions and groups ($\mathcal{C}' \cap \mathcal{C} = \emptyset$ and $\mathcal{K}' \cap \mathcal{K} = \emptyset$). Therefore, when making predictions with the training data, we must consider possible differences in the data distribution between training $\{(V'_j, Y'_j, C'_j, K'_j)\}_{j=1}^m$ and test $\{(V_i, Y_i, C_i, K_i)\}_{i=1}^n$.

Contributions. This paper makes the following contributions:

1. We explicitly define the statistical task of downstream inference about label prevalence $P(Y = 1|C = c)$ and the class-conditional means $\mathbb{E}[X|Y = y, C = c]$ using classification predictions. We codify the different sets of assumptions required to enable meaningful inference in this setting.
2. We develop semiparametric bootstrap methods for making downstream inference with classifier predictions, which properly incorporate variance when the required generalizability assumptions hold.
3. We demonstrate the use and performance of these methods in both simulation and in a detailed case study with TIRF microscopy data, where we describe the process of constructing a generalizable classifier, checking assumptions for valid statistical inference, and creating bootstrap confidence intervals.
4. Through our case study, we provide practical advice on feature and classifier construction in order to satisfy the assumptions necessary for downstream inference.

In Section 2, we describe previous literature on automatic labeling and generalizable classifiers. In Section 3, we present our bootstrap methods for inference with unlabeled data, and the different assumptions required. We demonstrate the performance of our methods on simulated data in Section 4, and discuss possible modifications of our algorithms for different scenarios. Finally, in Section 5, we perform inference in a case study with real TIRF microscopy data.

2 Background

2.1 Automated labeling in scientific studies

Automated labeling is useful in a wide range of applications, often with large image datasets. For example, Norouzzadeh et al. (2018) developed a classifier to identify animal species in camera trap images, as well as the number of animals in each picture and a description of their actions. The classifier was trained on millions of images from the Snapshot Serengeti dataset (Swanson et al., 2015), using convolutional neural networks. In ecology, large-scale classifiers have also been used to label deforestation (Maretto et al., 2020) and pest infestations (Rammer and Seidl, 2019). Automated labeling is also common in cell biology, where microscopy can produce thousands of images a day, which need to be annotated to identify nuclei (Caicedo et al., 2019), cell state and type (Christiansen et al., 2018), cell health phenotypes (Way et al., 2021), and protein localization (Kraus et al., 2017).

In each of these examples, it is important that classifiers generalize, or *transfer*, to new data. If predictions are not robust to changes in the distribution of input data, classifiers can fail when applied to new settings (Pan and Yang, 2009; Quiñonero-Candela et al., 2009). It has therefore become common for researchers constructing automated labeling systems to design classifiers which they expect to transfer. For example, Norouzzadeh et al. (2018) describe how their method can be updated for new camera trap locations with only a small amount of additional data.

2.2 Generalizable classifiers

A typical assumption in supervised learning is that training and test data come from the same distribution, which allows classifier predictions to be meaningful on new data. In practice, however, training and test data often come from different distributions, and so assumptions on the nature of distributional change are needed to understand how classifiers to generalize to new data.

Typically, we say that a classifier trained on data from condition $C = c'$, using the covariates V , generalizes to a new condition $C = c$ if $P(Y = y|V = v, C = c) = P(Y = y|V = v, C = c')$ (Subbaswamy et al., 2019). In this case, the features V satisfy the *covariate shift* assumption (Bickel et al., 2009; Gretton et al., 2009): the marginal distribution of V may change, but the conditional distribution of $Y|V$ remains the same. Under covariate shift, predictions can be applied directly to new data, or the classifier can be re-trained on weighted training data to be more efficient at risk minimization on test data (Shimodaira, 2000; Sugiyama et al., 2008). However, not all features typically satisfy the covariate shift assumption, as we expect systematic differences between conditions to appear in some features. Therefore, we write $V = \{X, Z, U\}$, where $X \in \mathbb{R}$ is a feature of interest for inference, U is a set of unused features, and $Z \in \mathbb{R}^d$ is a subset of covariates which satisfy the covariate shift assumption:

$$P(Y = y|Z = z, C = c) = P(Y = y|Z = z, C = c'), \quad \text{for all } c, c'. \quad (1)$$

Ideally, Z is also *sufficient* to capture the label information, so that $P(Y = y|X, U, Z, C) = P(Y = y|Z)$ (Peters et al., 2016; Kuang et al., 2018).

The strategy of identifying features that allow generalizability is common, and there are a variety of techniques. For example, Magliacane et al. (2017) and Rojas-Carulla et al. (2018) use variable selection techniques to identify a subset of predictors for which covariate shift holds, and Peters et al. (2016) performs hypothesis tests on the relationship between the predictors and the response. These methods are inspired by causal inference and causal discovery, as are Subbaswamy et al. (2019), who represent the data generating process explicitly with a causal graph and use the graph to identify stable predictors. Kuang et al. (2018) also use ideas from causal inference, in particular balancing models which use weights to account for differences in covariate distributions across environments, to identify a subset of covariates which generalize. More broadly,

other authors have developed regularized regression methods to learn features which are common to multiple environments (Argyriou et al., 2007, 2008).

In some cases, however, it may not be possible to identify an appropriate subset of features Z for which covariate shift holds (Subbaswamy et al., 2019). For example, if $Z|Y = y, C = c \stackrel{d}{=} Z|Y = y, C = c'$, but the prevalence $P(Y = y|C = c) \neq P(Y = y|C = c')$, then predicted probabilities will not be calibrated for all $c \in \mathcal{C}$. This is the *label shift* scenario, in which the marginal distribution of labels changes, but the conditional distributions of features remain the same. Fortunately, there are a variety of methods for detecting and correcting for label shift, which allow predictions to be easily adjusted in this setting (Saerens et al., 2002; Storkey, 2009; Lipton et al., 2018; Garg et al., 2020).

To accomodate situations like label shift, in this manuscript we consider a classifier trained on features Z to *generalize* if label probabilities $P(Y = y|Z = z, C = c)$ for each condition $c \in \mathcal{C}$ can be estimated from labeled training data $\{(Z'_j, Y'_j, C'_j, K'_j)\}_{j=1}^m$ and unlabeled test data $\{(Z_i, C_i, K_i)\}_{i=1}^n$ —either by directly applying a classifier, in the case of covariate shift, or by correcting classifier predictions, like in the case of label shift. The existence of appropriate features Z is assumed; in practice, there are a variety of methods for identifying Z , as discussed above, and in our case study on TIRF microscopy data we use simple exploratory techniques.

3 Inference with generalizable predictions

We are interested in two inference questions using the classifier labels. First, how label prevalence, $P(Y = y|C = c)$, differs across conditions C . Second, how the conditional distribution of a feature of interest X , $X|Y = y, C = c$, differs across conditions C . As the labels Y are unobserved for the new data, we use a classifier \mathcal{A} trained on labeled training data $\{(Z'_j, Y'_j, C'_j, K'_j)\}_{j=1}^m$. For simplicity, we'll assume that $Y \in \{0, 1\}$, so $\mathcal{A}(z) = \widehat{P}(Y' = 1|Z' = z)$, but the same methods can be used when labels belong to more than two classes. (Notation remark: training data is typically comprised of multiple conditions $C' \in \mathcal{C}'$, which may have different prevalences $P(Y' = 1|C')$. Probabilities which don't condition on C' , e.g. $P(Y' = 1)$, are understood to refer to the specific combination of conditions in the observed training data). To be able to make predictions on new data from new conditions $c \in \mathcal{C}$, we assume that our classifier generalizes, as discussed above in Section 2.2. In particular, we assume that the covariates Z satisfy the following assumptions:

(A1) $P(Y = 1|Z, C)$ can be estimated using the classifier \mathcal{A} , labeled training data $\{(Z'_j, Y'_j, C'_j, K'_j)\}_{j=1}^m$, and unlabeled test data $\{(Z_i, C_i, K_i)\}_{i=1}^n$.

(A2) $\mathcal{A}(z) = \widehat{P}(Y' = 1|Z' = z)$ is consistent for $P(Y' = 1|Z' = z)$.

If the features Z satisfy the covariate shift assumption, (A1) is straightforward, with $\widehat{P}(Y = 1|Z, C) = \mathcal{A}(Z)$. In other scenarios, classifier predictions $\mathcal{A}(Z)$ may need to be corrected on new data. For example, in the label shift setting, conditionwise prevalence $P(Y = 1|C = c)$ can be estimated for each condition $c \in \mathcal{C}$ using label shift correction methods (see Appendix A.1), and then $P(Y = 1|Z, C)$ is estimated via Bayes theorem:

$$\widehat{P}(Y = 1|Z, C) = \mathcal{A}_L(Z, C) := \frac{\frac{\widehat{P}(Y=1|C)}{\widehat{P}(Y'=1)} \mathcal{A}(Z)}{\frac{\widehat{P}(Y=1|C)}{\widehat{P}(Y'=1)} \mathcal{A}(Z) + \frac{1 - \widehat{P}(Y=1|C)}{1 - \widehat{P}(Y'=1)} (1 - \mathcal{A}(Z))}, \quad (2)$$

where $\mathcal{A}_L(Z, C)$ denotes the label shift-corrected predictions for condition C . For the purpose of this paper, we will focus on the label shift setting. However, we note that our work can be applied to other settings as well.

3.1 Inference for prevalence

Our first goal is to construct a confidence interval for the conditionwise prevalence, $P(Y = 1|C = c)$. Given estimated probabilities $\hat{P}(Y = 1|Z, C)$ that are close to the true probabilities $P(Y = 1|Z, C)$, point estimation of this quantity is straightforward: $\hat{P}(Y = 1|C = c) = \frac{1}{\#\{i:C_i=c\}} \sum_{i=1}^n \hat{P}(Y_i = 1|Z_i, C_i) \mathbb{1}\{C_i = c\}$.

Alternatively, in the label shift setting, $\hat{P}(Y = 1|C = c)$ is estimated separately by leveraging the label shift assumption (Appendix A.1). In either case, a simple binomial confidence interval for the prevalence $P(Y = 1|C = c)$ does not suffice, because $\hat{P}(Y = 1|C = c)$ relies on both training and test data. We therefore propose a bootstrap procedure which resamples both training and test data at each step. In particular, for bootstrap samples $s = 1, \dots, B$ we

1. Resample the training data, (Z_i^*, Y_i^{*s})
2. Retrain the classifier, \mathcal{A}^* , on the bootstrap training data
3. Resample the test data (Z_i^*, C_i^*)
4. Re-estimate the prevalence $\hat{P}(Y^* = 1|C^* = c)$

The full procedure, applied to the label shift setting, is described in Algorithm 2 in the Appendix. Algorithm 2 can also be easily modified for other forms of distributional change. For instance, in the case of covariate shift, we simply remove the label shift estimation and correction steps.

Similar bootstrap approaches are used below, for inference on $X|Y = y, C = c$. Here we make several remarks that apply to all the bootstrap procedures discussed in this paper.

Remark: Retraining a classifier on bootstrapped training data may be time-consuming. For certain classifiers, it may be possible to sample a new classification function without re-fitting the full model. For example, for a logistic GAM, penalizing the spline fit is equivalent to placing a prior distribution on the spline coefficients (Krivobokova et al., 2010; Wood, 2017). This results in a posterior distribution for the classifier function, given the training data, and this posterior distribution has good frequentist properties (Krivobokova et al., 2010). Then, a bootstrapped classifier \mathcal{A}^* can be sampled from this posterior distribution rather than by re-fitting on bootstrapped training data. Further details are provided in the Appendix.

Remark: Because estimates depend on both training and test data, our bootstrap procedure resamples both training and test. This also means that coverage for the resulting bootstrap confidence intervals is defined over pairs of training and test data $\{(Z'_i, Y'_i, C'_i, K'_i)\}, \{(Z_i, C_i, K_i)\}$. For example, if we construct a 95% confidence interval, in the long run 95% of training/test pairs $\{(Z'_i, Y'_i, C'_i, K'_i)\}, \{(Z_i, C_i, K_i)\}$ will produce an interval that captures the true parameter. It is *not* true that for any training set $\{(Z'_i, Y'_i, C'_i, K'_i)\}$, 95% of future test sets $\{(Z_i, C_i, K_i)\}$ will yield a confidence interval containing the true parameter.

Remark: Algorithm 2 (in the Appendix) describes a bootstrap procedure for confidence intervals. Here our bootstrap intervals are first order, such as bootstrap z -intervals, bootstrap percentile intervals, or bootstrap pivotal intervals. The same approach can be used for more accurate intervals, such as calibrated intervals, bootstrap t -intervals, and BC_a intervals (DiCiccio et al., 1996). However, these more accurate intervals require a second level of sampling at each bootstrap iteration, which is likely to be computationally infeasible with classifier retraining inside the bootstrap.

3.2 Inference for feature distributions

Our second question is how the conditional distribution of a feature of interest $X|Y = y, C = c$ differs across conditions c . We will focus on confidence intervals for the class-conditional mean $\mathbb{E}[X|Y = y, C = c]$, though

other summaries of the conditional distribution could be used instead. Given the hierarchical nature of the data, with grouping variables C and K , it is natural to model the conditional mean using a mixed effects model:

$$\mathbb{E}[X|Y = y, C = c, K = k] = \beta_{c,y} + b_k, \quad (3)$$

where $\beta_{c,y}$ is a fixed effect and $b_k \sim N(0, \omega^2)$ is a random effect.

The labels Y are unobserved, but we note that

$$\begin{aligned} \mathbb{E}[X|Y = y, C = c, K = k] &= \int x f_{X|Y=y,c,k}(x) dx = \int x \frac{P(Y = y|X = x, c, k)}{P(Y = y|c, k)} f_{X|c,k}(x) dx \\ &= \mathbb{E} \left[X \frac{P(Y = y|X, C = c, K = k)}{P(Y = y|C = c, K = k)} \middle| C = c, K = k \right]. \end{aligned} \quad (4)$$

Therefore, we can estimate $\beta_{c,y}$ in (3) using a weighted mixed effects model, where

$$X_i \sim N \left(\beta_{c_i,y} + b_{k_i}, \frac{\sigma_y^2}{w_{i,y}} \right), \quad b_k \sim N(0, \omega^2), \quad (5)$$

with weights $w_{i,y} = P(Y_i = y|X_i, C_i, K_i)$. The assumption of a parametric form for the random effect, which is used in bootstrapping, is necessary when we observe few levels of K for each condition C , which is common in many scientific studies. The assumption of conditional normality for the feature of interest X is used for maximum likelihood estimation (or restricted maximum likelihood estimation) of the model parameters, but is not required for inference. As we describe below, our approach to inference involves a semiparametric bootstrap which resamples residuals from the fitted model, and we see in simulations (Section 4) that departures from conditional normality do not seem to harm the coverage of our confidence intervals.

Since the true label probabilities $P(Y = y|X, C, K)$ are unknown, we use estimated probabilities instead, yielding weights $w_{i,y} = \hat{P}(Y_i = y|Z_i, C_i)$. This requires the assumption that the feature of interest X provides no additional information about the label Y , after accounting for the covariates Z and the condition C . Formally, we assume the following, which is similar to assumptions found in Peters et al. (2016) and Kuang et al. (2018):

$$(A3) \quad P(Y = y|X, Z, C, K) = P(Y = y|Z, C).$$

Fitting the model (5) with probability weights yields a point estimate $\hat{\beta}_{c,y}$. To construct a confidence interval for $\beta_{c,y}$, we bootstrap the training and test data, as in Section 3.1. When K has many levels for each $C = c$, then a hierarchical bootstrap may be employed to resample the test data. However, in many scientific studies, K often has few levels for each C , and so we instead create bootstrap test data by sampling random effects and residuals. In particular, we define residuals for each class $y \in \mathcal{Y}$ by $e_i = X_i - \hat{b}_{k_i}$, which we combine with new random effects $b_k^* \sim N(0, \hat{\omega}^2)$. In the context of label shift, for each bootstrap sample $s = 1, \dots, B$ we

1. Resample the training data, (Z_i^*, Y_i^*)
2. Retrain the classifier, \mathcal{A}^* , on the bootstrap training data
3. Resample the test data:
 - (a) Sample $b_k^* \sim N(0, \hat{\omega}^2)$ for each group $k \in \mathcal{K}$
 - (b) Sample $(Z_i^*, C_i^*, \mathcal{A}_L(Z_i^*, C_i^*), e_i^*)$ by resampling rows (to preserve any correlation between covariates Z and residuals e_i)
 - (c) Sample $Y_i^* \sim \text{Bernoulli}(\mathcal{A}_L(Z_i^*, C_i^*))$

- (d) Generate new observations X_i^* by $X_i^* = e_i^* + b_k^*$
4. Calculate the label shift correction on the bootstrap training and test data, and re-fit the weighted mixed effects model

The full details are provided in Algorithm 3 in the Appendix. As in Section 3.1, Algorithm 3 can be modified for other forms of distributional change. For covariate shift, simply remove the label shift correction steps, and replace $\mathcal{A}_L(Z, C)$ with $\mathcal{A}(Z)$.

Remark: Rather than probability weights, inference may also be based directly on binary predictions $\hat{Y}_i \in \{0, 1\}$. The procedure is similar, just with $\mathbb{E}[X|\hat{Y} = 1, C = c, K = k]$. If the classifier predictions $\mathcal{A}_L(Z, C)$ are good, we generally expect probability weights to give better estimates than binary predictions. In particular, if there is a relationship between X and $\mathcal{A}_L(Z, C)$, then thresholding classifier predictions to produce binary labels will lead to biased estimates.

Remark: A consequence of assumption (A3) is that the random effect b_k in (3) does not depend on the label Y . If random effects are in fact label-dependent, which may be assessed with training data, separate random effects can be estimated when fitting (5) and in constructing bootstrap confidence intervals. However, label-dependent random effects violate (A3) and so may lead to a decrease in confidence interval coverage. We investigate this further, and suggest a potential adjustment to improve coverage in Section 4.

3.3 Mixture models: an alternative to probability weighting

Assumption (A3) states that the covariates Z are sufficient for classification. This assumption can be checked on training data, but it may be challenging to find a subset of covariates Z which satisfies both (A3) and (A1), or even one which satisfies (A1) alone. In this case, estimating appropriate weights for the weighted mixed effects model (5) may be difficult. An alternative is to recognize that inference for the conditional feature distribution $X|Y = y, C = c$ naturally fits a mixture model approach, with the observed distribution of $X|C = c$ being a mixture of conditional distributions $X|Y = y, C = c$ over unobserved labels $y \in \mathcal{Y}$.

If $X|Y = y, C = c$ is assumed to follow a parametric distribution, then maximum likelihood estimation of the model parameters is possible. For example, we might assume a Gaussian hierarchical mixture where

$$X|Y = y, C = c, K = k \sim N(\beta_{c,y} + b_{k,y}, \sigma_y^2), \quad (6)$$

and $b_{k,y} \sim N(0, \omega_y^2)$. This replaces assumptions (A1) - (A3) with parametric assumptions on the conditional distribution of the feature of interest X ; while we use Gaussian mixture models throughout this paper, as in (6), other parametric distributions can be chosen based on the observed training data. Furthermore, by removing assumption (A3), it is straightforward to allow label-dependent random effects $b_{k,y}$ in (6). (*Note:* the parametric assumptions for the mixture model (5) are much more important for estimation than the parametric model used for mixed effect model estimation (6).)

However, mixture models can be difficult to estimate well, particularly when parametric assumptions are violated, and when the class distribution is unbalanced. To assist with mixture model estimation, we can use information from classifier predictions. In particular, we propose using a classifier to estimate $P(Y = y|C = c)$, and then using these class proportions to improve mixture model estimation. This approach relies on (A1) and (A2), but not (A3).

Thus we have two alternative assumptions for inference on the conditional mean $\mathbb{E}[X|Y = y, C = c]$: that Z is sufficient for classification (assumption (A3)), or that we know a parametric form for the conditional distribution $X|Y = y, C = c$ (as in (6)). Which assumption is more appropriate is problem-specific. The bootstrap procedure is almost identical to the one described in Section 3.2, the only difference is the model used for parameter estimation, and that residuals $e_{i,y}$ are calculated for each class to accommodate label-dependent random effects $b_{k,y}$. Algorithm 4, in the Appendix, describes the full procedure in detail in the context of label shift; as before, modifications are straightforward.

4 Simulations

In this section, we investigate the performance of the bootstrap procedures described in Section 3, using simulated data. All of our methods rely on some subset of: assumptions (A1), (A2), (A3), parametric assumptions about a feature X , and assumptions about the relationship between labels and random effects. To evaluate the impact of assumptions on the performance of our bootstrap methods, we assess coverage of bootstrap confidence intervals when different assumptions are satisfied.

As discussed in Section 3.1, inference for label prevalence requires assumptions (A1) and (A2), which allow label probabilities to be estimated on new data using a subset of covariates Z . For inference on a feature of interest X , we also require either assumption (A3) (if using the mixed effects approach of Section 3.2) or a known parametric form for the class distributions (if using the parametric mixture model approach of Section 3.3). To evaluate performance of our proposed confidence intervals, we consider six different simulation settings, varying the assumptions that are satisfied. For simplicity, we consider a single additional covariate Z , one test condition C ($|C| = 1$), and 15 nested subgroups K ($|\mathcal{K}| = 15$). As in the rest of this manuscript, we focus on label shift to illustrate our proposed procedures.

Scenarios. We consider three main scenarios, under which different combinations of (A1), (A2), and (A3) are satisfied. To evaluate the sensitivity of the mixture model approach to parametric assumptions, we use Gaussian mixture models and generate data from both Gaussian and skewed normal distributions for each scenario. The parameters of the skewed normal distributions are chosen so that variance and separation between the two class distributions are roughly equivalent to the Gaussian case. Full simulation details are provided in Table 5 in the Appendix.

Scenario 1: Assumptions (A1), (A2), and (A3) are satisfied. The covariate Z used for classification satisfies the label shift assumption between the training and test data (A1), and a logistic spline fit is used for classification (A2). Gaussian random effects b_k are generated for each $k \in \mathcal{K}$. The feature of interest X is given by $X_i = Z_i + b_{k_i} + \text{noise}$, satisfying (A3).

Scenario 2: Assumptions (A2) and (A3) are satisfied, but (A1) is not. Though label shift methods are employed for constructing confidence intervals, as in Algorithms 2, 3, and 4 (Appendix), the conditional distribution of $Z|Y = 0$ differs between training and test data. As in Scenario 1, a logistic spline fit is used for classification, and $X_i = Z_i + b_{k_i} + \text{noise}$.

Scenario 3: Assumptions (A1) and (A2) are satisfied, but (A3) is not. As in Scenario 1, the covariate Z satisfies the label shift assumption, and a logistic spline fit is used for classification. However, $\mathbb{E}[X|Z, Y = 1] \neq \mathbb{E}[X|Z, Y = 0]$, which violates (A3).

Comparisons. For each scenario, we calculate estimates and 95% confidence intervals for the prevalence $P(Y = 1|C = 1)$, and the class mean $\mathbb{E}[X|Y = 1, C = 1]$ (recall that for the test data, we consider only one test condition, i.e. $|C| = 1$). Inference for prevalence is done as in Section 3.1. Inference for $\mathbb{E}[X|Y = 1, C = 1]$ is done with both mixed effects models (Section 3.2) and mixture models (Section 3.3). Gaussian mixture models are used, and the mixing proportions are first estimated using label shift methods (Appendix A.1). As the random effect b_k in simulations does not depend on the class label Y , we modify Algorithm 4 to fit a single random effect for each $k \in \mathcal{K}$, as in Algorithm 3. We then compare the bias of the point estimates from each method, and the observed coverage of nominal 95% bootstrap pivotal intervals. Logistic splines were fit using the `mgcv` package (Wood, 2011) in `R`, while mixed effects models used the `lme4` package (Bates et al., 2015), and mixture models were implemented in `stan` using `rstan` (Stan Development Team, 2020).

Results. Average point estimates and confidence interval coverage are shown in Table 1. Inference for the prevalence $P(Y = 1|C = 1)$ depends on the validity of assumptions (A1) and (A2), and Table 1 shows that bias is small and coverage is close to the nominal level when (A1) and (A2) are satisfied, regardless of assumption (A3) and the parametric form of the data. The mixed effects model requires the additional assumption (A3) in order to perform inference on the feature of interest X . When (A1), (A2), and (A3)

are satisfied, bias is close to 0 and coverage is close to 95%, and this holds for both the normal and skewed normal distributions. However, when (A1) or (A3) are violated, the point estimates become biased, leading to a decrease in coverage. In contrast, the Gaussian mixture model requires (A1) and (A2), along with a feature X which is conditionally normal given class $y \in \mathcal{Y}$.

When these assumptions are met, bias and coverage both behave well. However, departures from normality lead to biased estimates and lower coverage. Violation of the label shift assumption also results in poor performance, because the label shift assumption is used to estimate mixing proportions.

Assumptions	Normal?	Prevalence		Mixed Effects Model		Mixture Model	
		Mean	Coverage	Mean	Coverage	Mean	Coverage
(A1), (A2), (A3)	yes	0.4 (0.001)	0.93 (0.015)	2.99 (0.008)	0.93 (0.014)	3 (0.007)	0.94 (0.013)
	no	0.4 (0.002)	0.9 (0.018)	3.51 (0.009)	0.93 (0.014)	3.86 (0.010)	0.28 (0.026)
(A2), (A3)	yes	0.35 (0.001)	0.07 (0.015)	3.16 (0.008)	0.72 (0.026)	3.13 (0.007)	0.8 (0.023)
	no	0.45 (0.002)	0.71 (0.026)	3.44 (0.009)	0.91 (0.016)	3.74 (0.009)	0.54 (0.029)
(A1), (A2)	yes	0.4 (0.001)	0.93 (0.015)	3.87 (0.008)	0.86 (0.020)	4 (0.007)	0.94 (0.014)
	no	0.4 (0.002)	0.9 (0.018)	4.12 (0.010)	0.41 (0.028)	4.68 (0.012)	0.63 (0.028)

Table 1: Coverage of bootstrap confidence intervals in simulated data.

4.1 Label-dependent random effects

As discussed in Section 3.2, the weighted mixed effects model (5) relies on assumption (A3) to use classifier predictions as probability weights. This assumes that the feature of interest, X , adds no information to the covariates Z to distinguish between labels $Y = 0$ and $Y = 1$. In practice, this may be true on average across the population but not within groups $k \in \mathcal{K}$. In particular, we may observe that the random effect b_k depends on both the group k and also the label Y , which violates (A3).

Label dependence can be accommodated in the mixed effects model by modifying Algorithm 3 to estimate separate separate random effects $b_{k,y}$ for $Y = 0$ and $Y = 1$ within each group $k \in \mathcal{K}$, as in Algorithm 4. Table 2 shows the results of mixed effects estimation and coverage. Here data is simulated as in Table 5, except that label-specific random effects $b_{k,y}$ are simulated separately for each $y \in \{0, 1\}$ (that is, $X_i = Z_i + b_{k,0}\mathbb{1}(Y_i = 0) + b_{k,1}\mathbb{1}(Y_i = 1) + \text{noise}$), and the model is fit by estimating each $b_{k,y}$ separately. Comparing Table 2 to Table 1, we see that while our point estimates perform equivalently, label dependence for the random effects results in decreased coverage for the confidence intervals.

This decrease in coverage arises because the probability weights in (5) are slightly wrong, which causes the random effect variance ω_y^2 to be underestimated. Fortunately, this issue can be corrected by an additional variance calibration step in the bootstrap. Let $\hat{\omega}_y^2$, $y \in \{0, 1\}$, be the initial variance estimates from fitting weighted mixed effects models. For bootstrap samples $s = 1, \dots, B$, we sample bootstrap training and test data as described in Algorithm 4, using our initial estimates $\hat{\omega}_y^2$. For each sample, we then calculate the observed variance estimate $\hat{\omega}_{y,s}^{*2}$. The same process that results in $\hat{\omega}_y^2$ being biased for ω_y^2 will cause $\hat{\omega}_{y,s}^{*2}$ to be biased for $\hat{\omega}_y^2$. Using the $\hat{\omega}_{y,s}^{*2}$ and $\hat{\omega}_y^2$, we estimate a variance correction, which we apply to $\hat{\omega}_y^2$. The corrected variance estimate is then used for bootstrap simulation to construct a confidence interval. Full details are provided in the Appendix.

Table 2 shows the estimates and coverage of the variance-adjusted mixed effects bootstrap. We can see that the bias remains the same, but adjusting the variance improves confidence interval coverage. For comparison, we also assess the Gaussian mixture model approach with label-dependent random effects (6). When all assumptions are satisfied, coverage of the mixture model confidence intervals is slightly worse than the variance-adjusted mixed effects approach, and is slightly worse than mixture model coverage in Table 1. This is because allowing label-dependent random effects increases the number of quantities to estimate in the mixture model, which makes model fitting more challenging.

Assumptions	Normal?	Mixed Effects Model		Mixed Effects, Variance Adjustment		Mixture Model	
		Mean	Coverage	Mean	Coverage	Mean	Coverage
(A1), (A2), (A3)	yes	3 (0.007)	0.91 (0.016)	3 (0.007)	0.94 (0.013)	3.01 (0.009)	0.89 (0.018)
	no	3.48 (0.007)	0.83 (0.022)	3.49 (0.006)	0.93 (0.015)	3.86 (0.008)	0.13 (0.020)
(A2), (A3)	yes	3.16 (0.008)	0.6 (0.028)	3.15 (0.008)	0.71 (0.026)	3.12 (0.008)	0.81 (0.022)
	no	3.45 (0.006)	0.91 (0.017)	3.42 (0.007)	0.89 (0.018)	3.75 (0.007)	0.37 (0.028)
(A1), (A2)	yes	3.88 (0.007)	0.78 (0.024)	3.89 (0.008)	0.84 (0.021)	4.01 (0.008)	0.86 (0.020)
	no	4.12 (0.007)	0.18 (0.022)	4.13 (0.008)	0.25 (0.025)	4.7 (0.009)	0.5 (0.029)

Table 2: Coverage of bootstrap confidence intervals in simulated data.

	Training data										
Condition	1	1	1	1	1	2	2	2	2	2	2
Cell	1-1	1-2	1-3	1-4	1-5	2-1	2-2	2-3	2-4	2-5	2-6
# Puffs	71	254	78	35	118	62	108	37	34	72	16
Puff prevalence	0.012	0.024	0.011	0.005	0.020	0.007	0.011	0.004	0.010	0.009	0.003

	Test data						
Condition	3	3	3	3	3	3	3
Cell	3-1	3-2	3-3	3-4	3-5	3-6	3-7
# Puffs	147	488	509	482	266	604	183
Puff prevalence	0.024	0.052	0.050	0.062	0.040	0.075	0.049

Table 3: Breakdown of events in each cell of the TIRF microscopy data, showing the number of puffs and the prevalence.

5 Case study: live cell microscopy data

In this section, we apply our methods for inference with classifier predictions to a large live cell microscopy dataset that was collected with TIRF microscopy and manually labeled. This will allow us to explore the process of assessing generalizability assumptions, engineering generalizable classifiers, and evaluating inference with unlabeled data.

Note: Aside from the issues we discuss in this paper, this TIRF dataset is known to have some human label bias. For illustrative purposes, we will ignore that label bias here and take the human labels as ground truth.

5.1 Data, classifier, and assumptions

Data. Labeled data was collected on TIRF microscopy images under three different experimental conditions, which we will refer to as Condition 1, Condition 2, and Condition 3, denoted respectively by $C = 1, 2, 3$. The experiment recorded data for 18 different cells, with 5 cells from Condition 1, 6 from Condition 2, and 7 from Condition 3, yielding a total of 134127 events across the 18 cells, with approximately 2.7% of the events being puffs.

Table 3 shows the breakdown of events in each cell. Conditions 1 and 2 have similar puff rates, while Condition 3 has a higher proportion of puffs, and furthermore it is hypothesized that puffs for Condition 3 may have different characteristics than puffs from Conditions 1 and 2. For this case study, we will therefore treat Conditions 1 and 2 as training data and Condition 3 as test data, allowing us to study generalization. For statistical inference, we want to construct confidence intervals for Condition 3. To reflect the process of classifier construction and assessment, we divide Conditions 1 and 2 into training data (7 cells) and validation data (4 cells). Note that the split between training and validation data is done by cell, to better capture cell-to-cell variability.

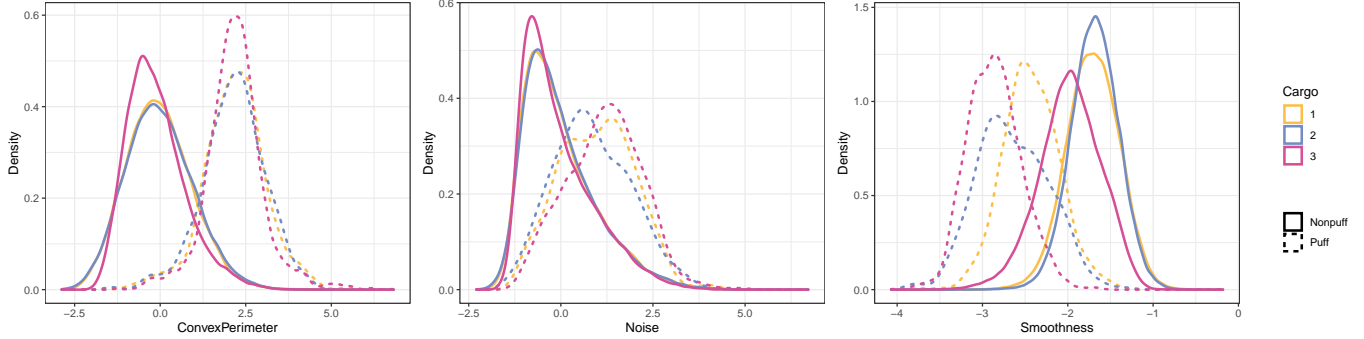


Figure 3: Distribution of three features calculated on the TIRF events, broken down by condition and puff/nonpuff. The first two features show label shift between the different conditions, and will be used to construct a classifier. The distribution of the third feature, *Smoothness*, changes between conditions. Inference on *Smoothness* in new conditions is of interest, but the feature is not included in the classifier because of the change in distribution.

Features. We will investigate the hypothesis that the pattern of diffusion into the cell membrane after vesicle fusion differs between conditions. To capture these diffusion differences, we create a feature called *Smoothness*, which we expect may vary across conditions. The feature is constructed using a functional PCA approach on the raw images (see Appendix) to capture a smoothness aspect of the diffusion. In the notation from Section 1, *Smoothness* is our feature of interest X .

We also construct a set of features Z for classification. These are carefully designed to capture the fundamental characteristics of puffs shown in Figure 1, and are also created from a functional PCA representation of the images (see Appendix). Because we expect common geometric characteristics of puffs to be preserved across conditions, but that the rate of puffs will differ, we will aim for generalizable prediction by constructing a set of features—and therefore a classifier—that obey the label shift assumption. We construct these by comparing the distributions of our designed features across conditions, selecting those features for which the label shift assumption appears to hold in exploratory data analysis. These are:

- *IntensityRatio*: the event’s maximum intensity / minimum intensity (Δ_f)
- *SNR*: a measure of the signal-to-noise in the event
- *ConvexArea* and *ConvexPerimeter*: measures of the amount of diffusion in the event’s intensity over time
- *Noise*: a measure of randomness in the event’s time series

For example, Figure 3 shows the distribution of *ConvexArea* and *ConvexPerimeter*; as the feature distribution within each class (puff and nonpuff) is the same between conditions, the only difference is one of label shift, which supports (A1). In contrast, the distribution of X (*Smoothness*) does not satisfy label shift, as expected (Figure 3).

To evaluate assumptions (A2) and (A3), we first need to construct a classifier.

Classifier. A logistic GAM (Hastie and Tibshirani, 1990; Wood, 2017) is trained on the seven training cells, using features $Z = \text{IntensityRatio}, \text{SNR}, \text{ConvexArea}, \text{ConvexPerimeter},$ and *Noise*. We choose a logistic GAM because it provides a balance between simplicity and flexibility, and because sampling from the posterior (see Appendix) makes our bootstrap procedures much more efficient. Performance of the classifier is assessed on the four validation cells, and the classifier is then applied to the test data. Use of validation data allows us to assess performance of classifier predictions on new data from the training distribution, which provides a benchmark for performance on new data from a different distribution. Figure 4 shows calibration plots for the predicted probabilities on validation and test data. As expected, the predicted probabilities

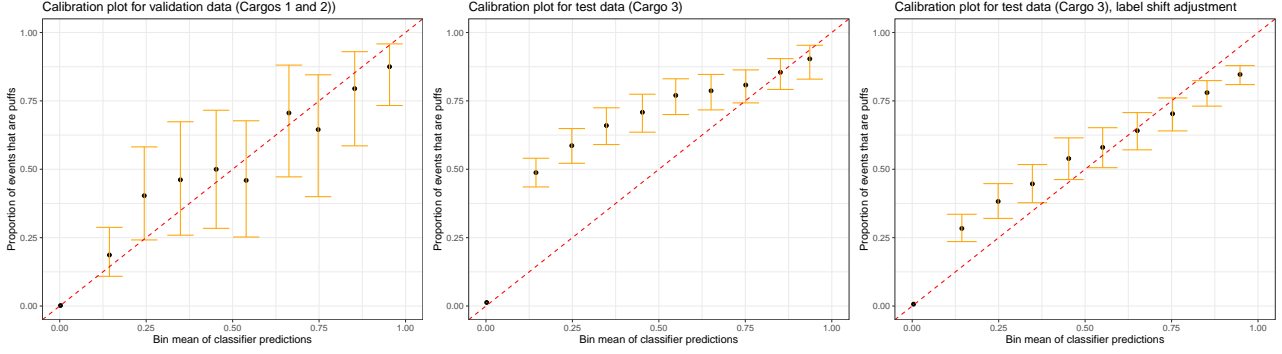


Figure 4: Calibration plots for the classifier on validation (left panel) and test data (middle and right panels). Because TfR cells have a higher proportion of puffs (Table 3), classifier predictions are mis-calibrated (middle panel), but they can be corrected with a label shift adjustment (right panel).

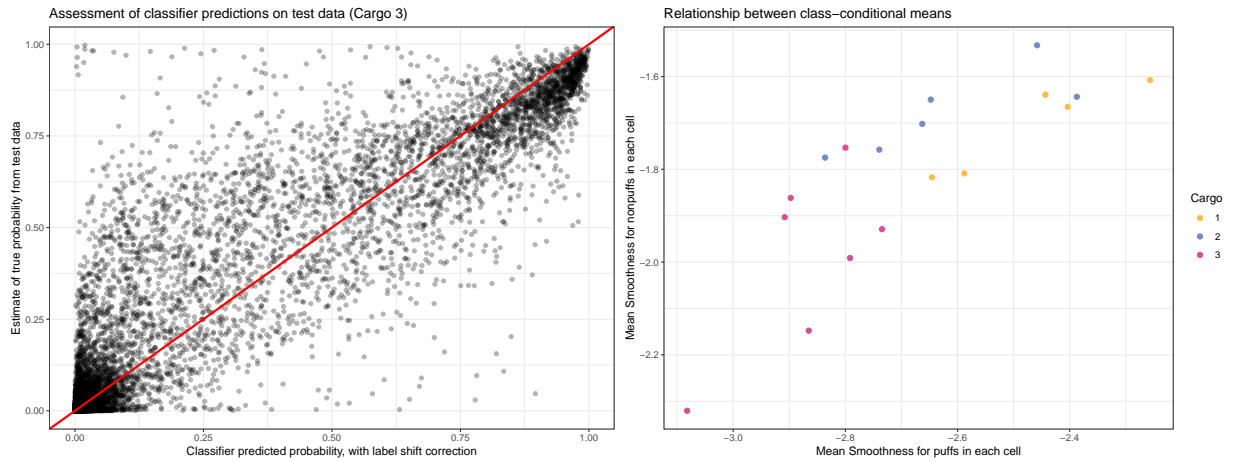


Figure 5: Left: $\hat{P}(Y_i = 1|X_i, Z_i)$ vs. $\mathcal{A}_L(Z_i, C_i)$ on test data. Right: Relationship between the class-conditional means $\mathbb{E}[X|Y = 1, C = c, K = k]$ and $\mathbb{E}[X|Y = 0, C = c, K = k]$ for each cell condition c and cell k .

appear to be calibrated on the validation data from Conditions 1 and 2 (which supports (A2)), but are mis-calibrated—due to label shift—on the test data from Condition 3. Furthermore, because the label shift assumption is appropriate for our classifier features (Figure 3), $P(Y = 1|C = 3)$ can be estimated as in the Appendix A.1. The resulting estimate is 0.043 using the method from Lipton et al. (2018), and 0.050 using the fixed point method based on Saerens et al. (2002) (Section 5.2), compared to the true sample prevalence of 0.051. Using this estimate, we correct the classifier predictions as in (2) with Bayes theorem, and Figure 4 shows the corrected predictions are much better calibrated, which again supports (A1).

Finally, to conduct inference about $X|Y = y, C = c$, we require (A3) to hold. To assess (A3), we compare $\mathcal{A}_L(Z, C)$ from (2) to an estimate of $P(Y = 1|X, Z, C)$ from regression on the test data. The resulting plot is shown in Figure 5, which suggests that while not perfect, the corrected predictions $\mathcal{A}_L(Z, C)$ are a good estimate of the true probability $P(Y = 1|X, Z, C)$. As discussed in Section 3 and Section 4, a consequence of (A3) is that the per-cell random effect b_k should not depend on the label Y . Figure 5 also shows the relationship between $\mathbb{E}[X|Y = 1, C = c, K = k]$ and $\mathbb{E}[X|Y = 0, C = c, K = k]$. As the relationship is roughly linear with a slope of approximately 1, the assumption of label-independent random effects is not unreasonable, but confidence intervals can also be constructed that model label-dependent random effects if desired, as described in Section 4.

Cell	Puff mean	Weighted mean, raw	Weighted mean, label shift	Threshold mean, raw	Threshold mean, label shift	Nonpuff mean
3-1	-3.08	-3.09	-3.01	-3.19	-3.11	-2.32
3-2	-2.90	-2.97	-2.84	-3.10	-2.99	-1.86
3-3	-2.91	-2.95	-2.86	-3.05	-2.94	-1.90
3-4	-2.87	-2.99	-2.92	-3.10	-2.99	-2.15
3-5	-2.80	-2.92	-2.82	-3.06	-2.94	-1.75
3-6	-2.79	-2.92	-2.85	-3.04	-2.93	-1.99
3-7	-2.73	-2.78	-2.67	-2.90	-2.77	-1.93
Combined	-2.87	-2.95	-2.85	-3.06	-2.95	-1.99

Table 4: Performance of estimates with classifier predictions on test data (Condition 3).

5.2 Inference with classifier predictions

Inference for prevalence. We begin with inference for $P(Y = 1|C = 3)$. Our point estimate, from label shift estimation, was 0.050 using the fixed point method (see Saerens et al. (2002) and Appendix A.1) and 0.043 using the method from Lipton et al. (2018). Using the procedure described in Algorithm 2, we construct a 95% confidence interval for $P(Y = 1|C = 3)$ with each label shift method, which are respectively (0.047, 0.055) and (0.039, 0.049). Both label shift estimates are a marked improvement on the point estimate from uncorrected classifier probabilities, which is 0.029.

To assess coverage of this interval, we perform a simulation using the real TIRF microscopy data. We simulate new training and test sets by resampling from the original training and test data, using Algorithm 2 to calculate a bootstrap confidence interval for the prevalence $P(Y = 1|C = 3)$ in each simulation. The simulated training data ($C = 1, 2$) has a prevalence of 0.01, while the simulated test data ($C = 3$) has a prevalence of 0.05. Using the fixed point method (Appendix A.1 and Saerens et al. (2002)), nominal 95% bootstrap pivotal intervals have a coverage of 95% in simulations, while coverage using the discretization method (Lipton et al., 2018) is about 19%. The lower coverage using the discretization method is due to bias, which may result because the prevalences are close to 0, or because the label shift assumption is not perfectly satisfied.

Inference for feature distributions. Next, we are interested in constructing a confidence interval for $\mathbb{E}[X|Y = 1, C = 3]$, where X is diffusion *Smoothness*. We first examine estimates of mean puff *Smoothness* in each test cell, using classifier predictions. Table 4 shows estimates using both probability weights and binary predictions from thresholding, and compares the classifier with and without label shift correction. We can see that the estimated means are close to the true sample means in each cell, and as expected the label shift correction produces better estimates. The weighted mean generally does better than the thresholding-based mean, which is biased because classifier predictions are negatively associated with *Smoothness*.

The point estimate for $\mathbb{E}[X|Y = 1, C = 3]$, using the weighted mixed effects model (5), is -2.85. Using the procedure described in Algorithm 3, we construct a confidence interval, which is (-3.00, -2.73). To assess coverage of our confidence interval on TIRF microscopy data, we simulate new training and test sets from the real data. Training data is sampled by bootstrapping from the original training data, and test data is simulated by adding a per-cell random effect to *Smoothness* in bootstrap samples from the original test data. For each simulated training and test pair, the procedure in Algorithm 3 is used to construct a confidence interval, and coverage is assessed across training/test pairs. In these simulations, nominal 95% bootstrap pivotal intervals have a coverage of about 90%, with similar numbers for other first-order intervals like bootstrap percentile intervals. This is close to the coverage seen in our simulations in Section 4.

Using a modification of Algorithm 3 to accommodate label-dependent random effects, a 95% bootstrap confidence interval for $\mathbb{E}[X|Y = 1, C = 3]$ in the test data is (-2.93, -2.78). In simulations with label-dependent random effects, these nominal 95% intervals again have a coverage of about 90%. The difference in width between the two confidence intervals likely results from different estimates of the random effect variance: as

the nonpuff cell means vary slightly more than the puff cell means in the observed data, bootstrap puff data varies less when we allow label-dependent random effects.

Mixture models. As an alternative to probability weighting, we employ the mixture model approach described in Section 3.3. We use a two-component Gaussian mixture, fitting the hierarchical mixture described in (6). To improve estimation of the mixture model, we pre-specify the prevalence of puffs in the test data, using the label shift estimate that we calculated above. Our point estimate for $\mathbb{E}[X|Y = 1, C = 3]$ is then $\hat{\beta}_{3,1} = -2.95$, and the confidence interval from Algorithm 4 is $(-2.99, -2.85)$. To assess coverage, we simulate from training/test pairs as with the mixed effects model above. Even though pre-specifying the puff prevalence improves the mixture estimation, the nominal 95% bootstrap percentile intervals have a coverage of approximately 15%. The poor coverage here is due largely to bias resulting from skewness in the data, which matches the simulation results for the skewed normal distribution in Section 4. We experimented with other parametric models beyond a Gaussian mixture, but estimation remained challenging. Figures showing the fitted Gaussian mixture model in each cell (with and without pre-specifying puff prevalence) can be found in the Appendix, in addition to the estimated means in each cell.

6 Discussion

Scientific studies often require painstakingly labeling large volumes of unlabeled data, causing labeling to be a key limiting factor in data analysis. If data can be automatically labeled with predictive models, manual labeling costs can be dramatically reduced and much higher through-put science can be enabled. However, rigorous scientific analysis with predicted labels requires generalizable classifier predictions for valid inference.

We have described methods for valid inference two common downstream targets of inference: the label prevalence $P(Y = y|C = c)$ and class-conditional feature means $\mathbb{E}[X|Y = y, C = c]$. Inspired by our motivating example from TIRF microscopy, we focus on the case where the classifier used for automatic labeling is trained on data that differs in distribution from the new, unlabeled data. As this dataset shift may prevent classifiers from generalizing to the new data, and therefore prevent valid statistical inference, we rely on identification of a subset of features that enable construction of a generalizable classifier. These features can be designed from training data, and a variety of methods exist to construct features which satisfy the covariate shift assumption (Peters et al., 2016; Magliacane et al., 2017; Kuang et al., 2018; Rojas-Carulla et al., 2018; Subbaswamy et al., 2019). In our TIRF microscopy case study, a label shift assumption is more appropriate than covariate shift, and we show that exploratory data analysis and careful feature engineering can construct generalizable covariates.

While we focus on the label shift setting in our algorithms, simulations, and case study, our methods can be easily modified for other types of dataset shift. Furthermore, our methods are designed to accommodate a flexible hierarchical data structure, which is common to scientific experiments in which multiple repetitions of the experiment are performed for each experimental condition. Through simulations and a case study with TIRF microscopy data, we show that the tools presented in this manuscript allow statistical inference with unlabeled, classifier-scored data, and that a generalizable classifier is crucial for valid analysis.

For inference with the class-conditional means $\mathbb{E}[X|Y = y, C = c]$, we describe two approaches for using classifier predictions for estimation and confidence intervals: weighted mixed effects models that use classifier predictions as probability weights, and hierarchical mixture models that use classification to estimate mixing proportions. The specific assumptions required by these two approaches are detailed in Section 3.2 and Section 3.3. As seen in simulations and the TIRF microscopy case study, the weighted mixed effects method is particularly sensitive to violations of assumption (A3), that the feature of interest X does not help distinguish between the classes $y \in \mathcal{Y}$ once we condition on the classifier features Z . On the other hand, the mixture model method is particularly sensitive to departures from the assumed parametric class distributions. Which assumption is more appropriate is problem dependent; fortunately, though assumptions typically cannot be checked on test data, they can be assessed on training data. As a result, collecting a large and diverse

training set, with observations from many domains, is an important part of data analysis.

The methods we propose in this manuscript allow valid statistical inference under appropriate assumptions, but there are still limitations to inference on unlabeled data. Even if classifier generalizability assumptions hold for inference on some features of interest, they may fail for others. In other cases, it may be impossible to construct features which satisfy the necessary conditions. Interpretation of inference results is also more nuanced: since confidence intervals must account for variability in the training data, coverage applies to joint training/test pairs, rather than to all new test datasets. Even more subtly, we often rely on humans to provide “ground truth” labels for classifier training; however, if researchers are accustomed to labeling observations under only some experimental conditions, then manual labels may suffer the same generalizability problems as automated predictions. While the methods in this paper may not help generalize human predictions, we believe that the explicit assumptions discussed above can still help researchers reflect on their own manual labeling system.

Acknowledgments

The authors would like to thank Hao Chen, Jennifer M. Kunselman, and Stephanie E. Crilly for advice and assistance, and Alexandra Chouldechova for computational resources. This work was supported by NSF DMS1613202 (CE and MG), NIH K12GM081266 (ZYW), and NIH GM117425 (MAP).

References

- Argyriou, A., Evgeniou, T., and Pontil, M. (2008). Convex multi-task feature learning. *Machine learning*, 73(3):243–272.
- Argyriou, A., Micchelli, C. A., Pontil, M., and Ying, Y. (2007). A spectral regularization framework for multi-task structure learning. In *NIPS*, volume 1290, page 1296. Citeseer.
- Axelrod, D. (1981). Cell-substrate contacts illuminated by total internal reflection fluorescence. *The Journal of Cell Biology*, 89(1):141–145.
- Bates, D., Mächler, M., Bolker, B., and Walker, S. (2015). Fitting linear mixed-effects models using lme4. *Journal of Statistical Software*, 67(1):1–48.
- Bickel, S., Brückner, M., and Scheffer, T. (2009). Discriminative learning under covariate shift. *Journal of Machine Learning Research*, 10(9).
- Bohannon, K. P., Bittner, M. A., Lawrence, D. A., Axelrod, D., and Holz, R. W. (2017). Slow fusion pore expansion creates a unique reaction chamber for co-packaged cargo. *The Journal of general physiology*, 149(10):921–934.
- Bowman, S. L., Soohoo, A. L., Shiwarski, D. J., Schulz, S., Pradhan, A. A., and Puthenveedu, M. A. (2015). Cell-autonomous regulation of mu-opioid receptor recycling by substance p. *Cell reports*, 10(11):1925–1936.
- Caicedo, J. C., Goodman, A., Karhohs, K. W., Cimini, B. A., Ackerman, J., Haghighi, M., Heng, C., Becker, T., Doan, M., McQuin, C., et al. (2019). Nucleus segmentation across imaging experiments: the 2018 data science bowl. *Nature methods*, 16(12):1247–1253.
- Christiansen, E. M., Yang, S. J., Ando, D. M., Javaherian, A., Skibinski, G., Lipnick, S., Mount, E., O’Neil, A., Shah, K., Lee, A. K., et al. (2018). In silico labeling: predicting fluorescent labels in unlabeled images. *Cell*, 173(3):792–803.
- DiCiccio, T. J., Efron, B., et al. (1996). Bootstrap confidence intervals. *Statistical science*, 11(3):189–228.

- Garg, S., Wu, Y., Balakrishnan, S., and Lipton, Z. C. (2020). A unified view of label shift estimation. *arXiv preprint arXiv:2003.07554*.
- Gretton, A., Smola, A., Huang, J., Schmittfull, M., Borgwardt, K., and Schölkopf, B. (2009). Covariate shift by kernel mean matching. *Dataset shift in machine learning*, 3(4):5.
- Hastie, T. J. and Tibshirani, R. J. (1990). *Generalized additive models*, volume 43. CRC press.
- Kou, Z. W., Mo, J. L., Wu, K. W., Qiu, M. H., Huang, Y. L., Tao, F., Lei, Y., Lv, L. L., and Sun, F. Y. (2019). Vascular endothelial growth factor increases the function of calcium-impermeable AMPA receptor GluA2 subunit in astrocytes via activation of protein kinase C signaling pathway. *Glia*, 67(7):1344–1358.
- Kraus, O. Z., Grys, B. T., Ba, J., Chong, Y., Frey, B. J., Boone, C., and Andrews, B. J. (2017). Automated analysis of high-content microscopy data with deep learning. *Molecular systems biology*, 13(4):924.
- Krivobokova, T., Kneib, T., and Claeskens, G. (2010). Simultaneous confidence bands for penalized spline estimators. *Journal of the American Statistical Association*, 105(490):852–863.
- Kuang, K., Cui, P., Athey, S., Xiong, R., and Li, B. (2018). Stable prediction across unknown environments. In *Proceedings of the 24th ACM SIGKDD International Conference on Knowledge Discovery & Data Mining*, pages 1617–1626.
- Lipton, Z. C., Wang, Y.-X., and Smola, A. (2018). Detecting and correcting for label shift with black box predictors. *arXiv preprint arXiv:1802.03916*.
- Logan, T., Bendor, J., Toupin, C., Thorn, K., and Edwards, R. H. (2017). α -Synuclein promotes dilation of the exocytotic fusion pore. *Nature Neuroscience*, 20(5):681–689.
- Magliacane, S., van Ommen, T., Claassen, T., Bongers, S., Versteeg, P., and Mooij, J. M. (2017). Domain adaptation by using causal inference to predict invariant conditional distributions. *arXiv preprint arXiv:1707.06422*.
- Maretto, R. V., Fonseca, L. M., Jacobs, N., Körting, T. S., Bendini, H. N., and Parente, L. L. (2020). Spatio-temporal deep learning approach to map deforestation in amazon rainforest. *IEEE Geoscience and Remote Sensing Letters*.
- Norouzzadeh, M. S., Nguyen, A., Kosmala, M., Swanson, A., Palmer, M. S., Packer, C., and Clune, J. (2018). Automatically identifying, counting, and describing wild animals in camera-trap images with deep learning. *Proceedings of the National Academy of Sciences*, 115(25):E5716–E5725.
- Pan, S. J. and Yang, Q. (2009). A survey on transfer learning. *IEEE Transactions on knowledge and data engineering*, 22(10):1345–1359.
- Peters, J., Bühlmann, P., and Meinshausen, N. (2016). Causal inference by using invariant prediction: identification and confidence intervals. *Journal of the Royal Statistical Society. Series B (Statistical Methodology)*, pages 947–1012.
- Pippig, S., Andexinger, S., and Lohse, M. J. (1995). Sequestration and recycling of beta 2-adrenergic receptors permit receptor resensitization. *Molecular Pharmacology*, 47(4):666–676.
- Quiñonero-Candela, J., Sugiyama, M., Lawrence, N. D., and Schwaighofer, A. (2009). *Dataset shift in machine learning*. Mit Press.
- Rammer, W. and Seidl, R. (2019). Harnessing deep learning in ecology: An example predicting bark beetle outbreaks. *Frontiers in plant science*, 10:1327.
- Ramsay, J. and Silverman, B. (2005). *Functional data analysis*. Springer.
- Rappoport, J. Z., Taha, B. W., Lemeer, S., Benmerah, A., and Simon, S. M. (2003). The AP-2 Complex Is Excluded from the Dynamic Population of Plasma Membrane-associated Clathrin. *Journal of Biological Chemistry*, 278(48):47357–47360.

- Rojas-Carulla, M., Schölkopf, B., Turner, R., and Peters, J. (2018). Invariant models for causal transfer learning. *The Journal of Machine Learning Research*, 19(1):1309–1342.
- Saerens, M., Latinne, P., and Decaestecker, C. (2002). Adjusting the outputs of a classifier to new a priori probabilities: a simple procedure. *Neural computation*, 14(1):21–41.
- Sankaranarayanan, S., De Angelis, D., Rothman, J. E., and Ryan, T. a. (2000). The Use of pHluorins for Optical Measurements of Presynaptic Activity. *Biophysical Journal*, 79(4):2199–2208.
- Shimodaira, H. (2000). Improving predictive inference under covariate shift by weighting the log-likelihood function. *Journal of statistical planning and inference*, 90(2):227–244.
- Stan Development Team (2020). RStan: the R interface to Stan. R package version 2.21.2.
- Storkey, A. (2009). When training and test sets are different: characterizing learning transfer. *Dataset shift in machine learning*, pages 3–28.
- Subbaswamy, A., Schulam, P., and Saria, S. (2019). Preventing failures due to dataset shift: Learning predictive models that transport. In *The 22nd International Conference on Artificial Intelligence and Statistics*, pages 3118–3127. PMLR.
- Sugiyama, M., Suzuki, T., Nakajima, S., Kashima, H., von Bünau, P., and Kawanabe, M. (2008). Direct importance estimation for covariate shift adaptation. *Annals of the Institute of Statistical Mathematics*, 60(4):699–746.
- Swanson, A., Kosmala, M., Lintott, C., Simpson, R., Smith, A., and Packer, C. (2015). Snapshot serengeti, high-frequency annotated camera trap images of 40 mammalian species in an african savanna. *Scientific data*, 2(1):1–14.
- Way, G. P., Kost-Alimova, M., Shibue, T., Harrington, W. F., Gill, S., Piccioni, F., Becker, T., Shafqat-Abbasi, H., Hahn, W. C., Carpenter, A. E., et al. (2021). Predicting cell health phenotypes using image-based morphology profiling. *Molecular Biology of the Cell*, 32(9):995–1005.
- Wood, S. N. (2011). Fast stable restricted maximum likelihood and marginal likelihood estimation of semi-parametric generalized linear models. *Journal of the Royal Statistical Society (B)*, 73(1):3–36.
- Wood, S. N. (2017). *Generalized additive models: an introduction with R*. CRC press.
- Yu, S. S., Lefkowitz, R. J., and Hausdorff, W. P. (1993). Beta-adrenergic receptor sequestration. A potential mechanism of receptor resensitization. *Journal of Biological Chemistry*, 268(1):337–341.
- Yudowski, G. A., Puthenveedu, M. A., and von Zastrow, M. (2006). Distinct modes of regulated receptor insertion to the somatodendritic plasma membrane. *Nature neuroscience*, 9(5):622–627.

A Appendix

A.1 Label shift estimation

Let $\{(Z'_i, Y'_i, C'_i)\}_{i=1}^m$ denote a set of labeled training data, and $\{(Z_j, C_j)\}_{j=1}^n$ a set of unlabeled test data with unobserved labels $Y_j \in \{0, 1\}$. Let \mathcal{A} denote a classifier fit on the training data, with $\mathcal{A}(z) = \widehat{P}(Y'_i = 1 | Z'_i = z)$. Under the label shift assumption, $P(Y = 1 | Z = z, C = c) \neq P(Y' = 1 | Z' = z, C' = c')$, and classifier predictions $\mathcal{A}(z)$ must be corrected to $\mathcal{A}_L(z, c)$ by equation (2).

This requires estimating the prevalence $P(Y = 1 | C = c)$ for each $c \in \mathcal{C}$, which is challenging when labels are unobserved. Fortunately, the test prevalence $P(Y = 1 | C = c)$ can be estimated under the label shift assumption. Here we summarize two different approaches, which in our experience are simple but generally reliable for label shift estimation.

A.1.1 Discretization method

The discretization approach is due to Lipton et al. (2018), and we summarize the method in Algorithm 1. Their approach relies on discretizing the predicted probabilities $\mathcal{A}(Z)$, and recognizing that under label shift $\mathcal{A}(Z) \perp\!\!\!\perp C|Y$.

Algorithm 1: Discretization method for label shift prevalence estimation (Lipton et al., 2018)

Data: Labeled training data $\{(Z'_i, Y'_i, C'_i)\}_{i=1}^m$

Unlabeled test data $\{(Z_j, C_j)\}_{j=1}^n$

Classifier \mathcal{A} with $\mathcal{A}(z) = \hat{P}(Y'_i = 1|Z'_i = z)$

Input : Discretization threshold $h \in (0, 1)$

Output: Estimated prevalence $\hat{P}(Y = 1|C = c)$ for each $c \in \mathcal{C}$

init

 Calculate discretized predictions on training data: $\hat{Y}'_i = \mathbb{1}\{\mathcal{A}(Z'_i) > h\}$;

 Calculate discretized predictions on test data: $\hat{Y}_j = \mathbb{1}\{\mathcal{A}(Z_j) > h\}$;

for $c \in \mathcal{C}$ **do**

$\boldsymbol{\pi}_{train} = \left[\frac{1}{m} \sum_{i=1}^m (1 - Y'_i), \frac{1}{m} \sum_{i=1}^m Y'_i \right]^T$;

$\mathbf{M} \in \mathbb{R}^{2 \times 2}$, with $M_{ij} = \frac{1}{m} \sum_{k=1}^m \mathbb{1}\{\hat{Y}'_k = i - 1, Y'_k = j - 1\}$, for $i, j \in \{1, 2\}$;

$\hat{\boldsymbol{\pi}}_{test} = \left[\frac{1}{\#\{i: C_i = c\}} \sum_{j=1}^n (1 - \hat{Y}_j) \mathbb{1}\{C_j = c\}, \frac{1}{\#\{i: C_i = c\}} \sum_{j=1}^n \hat{Y}_j \mathbb{1}\{C_j = c\} \right]^T$;

$\hat{P}(Y = 1|C = c) = (\mathbf{M}^{-1} \hat{\boldsymbol{\pi}}_{test})[2] \cdot \boldsymbol{\pi}_{train}[2]$, where $\boldsymbol{v}[2]$ denotes the second element of vector \boldsymbol{v} ;

end

return $\hat{P}(Y = 1|C = c)$ for each $c \in \mathcal{C}$

A.1.2 Fixed point method

The discretization method converts predicted probabilities in $(0, 1)$ to binary predictions by thresholding. This requires specifying a threshold, and the choice of threshold may impact the resulting prevalence estimates, particularly if the label shift assumption holds only approximately or there are few observations from one class. An alternative is to consider the label shift corrected probabilities $\mathcal{A}_L(z, c)$, calculated from $\mathcal{A}(z)$ via Bayes theorem (2).

Let $\pi_{test,c}$ be a putative value for $P(Y = 1|C = c)$, and $\mathcal{A}_L^{\pi_{test,c}}(z, c)$ the corrected probabilities using $\pi_{test,c}$ in (2). If \mathcal{A} is a calibrated classifier on the training data, and $\pi_{test,c}$ is close to $P(Y = 1|C = c)$, then under the label shift assumption $\pi_{test,c} \approx \frac{1}{\#\{i: C_i = c\}} \sum_{j=1}^n \mathcal{A}_L^{\pi_{test,c}}(Z_j, C_j) \mathbb{1}\{C_j = c\}$. The fixed point method considers a range $[a, b] \subset (0, 1)$ of potential values for $P(Y = 1|C = c)$, and estimates prevalence by

$$\hat{P}(Y = 1|C = c) = \arg \min_{\pi_{test,c} \in [a,b]} \left| \frac{1}{\#\{i: C_i = c\}} \sum_{j=1}^n \mathcal{A}_L^{\pi_{test,c}}(Z_j, C_j) \mathbb{1}\{C_j = c\} - \pi_{test,c} \right|. \quad (7)$$

(The restricted range $[a, b]$ is required to avoid trivial solutions). This is essentially the approach proposed by Saerens et al. (2002), just implemented as a search rather than through iterated EM updates.

A.2 Posterior sampling for logistic GAMs

The inference procedure described in Section 3 requires the ability to sample a new classifier function \mathcal{A}^* at each bootstrap step. As bootstrapping the training data and refitting the classifier at each step is

potentially very computationally expensive, it may be necessary to use a classifier for which the variability is understood. In particular, we want to resample the full classification function at every step, not just characterize variability at a single point (this requirement is sufficient to construct global confidence bands for the probability function, not just pointwise confidence intervals). As an example, we show here how standard results for logistic GAMs can be incorporated into the bootstrap procedure described above.

Letting Z_1, \dots, Z_d denote the components of Z , the logistic GAM models $P(Y = 1|Z)$ by

$$\text{logit } P(Y = 1|Z) = f_1(Z_1) + \dots + f_d(Z_d), \quad (8)$$

where f_1, \dots, f_d are smooth functions (Hastie and Tibshirani, 1990; Wood, 2017). The model is estimated with a spline fit. Let $\bar{\mathbf{Z}}$ be the design matrix for the spline fit (capturing the intercept and Z), let $\boldsymbol{\beta}$ be the spline coefficients, and λ the smoothing parameter. The spline fit is penalized by $\lambda \boldsymbol{\beta}^T \mathbf{S} \boldsymbol{\beta}$ where λ is the smoothing parameter and \mathbf{S} is the spline smoothing matrix; for example, for smoothing splines $\lambda \boldsymbol{\beta}^T \mathbf{S} \boldsymbol{\beta}$ corresponds to a penalty on the integrated squared second derivative of the smooth. It turns out that this penalty term is equivalent to using the prior distribution $\boldsymbol{\beta} | \lambda \sim N(\mathbf{0}, (\lambda \mathbf{S})^-)$, where $(\lambda \mathbf{S})^-$ denotes the pseudo-inverse (Wood, 2017). The posterior distribution of $\boldsymbol{\beta}$, given the training data (X'_i, Z'_i, Y'_i) , is approximately

$$\boldsymbol{\beta} | \{(Z'_i, Y'_i)\}_{i=1}^m, \lambda \sim N(\hat{\boldsymbol{\beta}}, (\bar{\mathbf{Z}}^T \mathbf{W} \bar{\mathbf{Z}} + \lambda \mathbf{S})^{-1}), \quad (9)$$

where $\hat{\boldsymbol{\beta}}$ are the estimated coefficients and \mathbf{W} is the weights matrix from the last step of penalized iterative reweighted least squares estimation (Wood, 2017).

If we use a logistic GAM as our classifier, we can draw a new classifier function \mathcal{A}^* in the bootstrap procedure discussed above by sampling from the posterior distribution of $\boldsymbol{\beta}$. While we expect draws from a posterior to give Bayesian credible intervals, posteriors for spline fits often have good frequentist properties (Krivobokova et al., 2010; Wood, 2017), and so it is reasonable to sample from the posterior in (9) to construct our frequentist bootstrap confidence intervals.

A.3 Bootstrap algorithms for inference

In Section 3, we describe semiparametric bootstrap procedures for inference with prevalence $P(Y = y|C = c)$ and class-conditional feature means $\mathbb{E}[X|Y = y, C = c]$. Here we include the detailed algorithms for implementing each bootstrap procedure. Algorithm 2 describes the procedure from Section 3.1 for constructing a confidence interval for prevalence; Algorithm 3 constructs confidence intervals for $\mathbb{E}[X|Y = y, C = c]$ using probability-weighted mixed effects models, as in Section 3.2; and Algorithm 4 constructs confidence intervals for $\mathbb{E}[X|Y = y, C = c]$ using parametric mixture models assisted by label shift estimation, as in Section 3.3.

A.4 Mixed effects models with label-dependent random effects

As we discuss in Section 3 and Section 4, confidence intervals from the weighted mixed effects model (5) may lose coverage when random effects are label dependent. In Table 2, we saw this decrease in coverage, and also that an additional variance calibration step can address the issue. Algorithm 5 details the full mixed effects procedure when random effects are label-dependent, including the variance calibration step. Note that variance calibration approximately doubles the time needed to construct a bootstrap confidence interval.

A.5 Simulation settings

In Section 4, we conduct simulations to assess the impact of assumptions on the coverage of our bootstrap confidence intervals. We describe three different scenarios, with different combinations of (A1), (A2), and

Algorithm 2: Semiparametric bootstrap confidence intervals for prevalence, under label shift

Data: Labeled training data $\{(Z'_i, Y'_i, C'_i, K'_i)\}_{i=1}^m$

Unlabeled test data $\{(Z_j, C_j, K_j)\}_{j=1}^n$

Input : Number B of bootstrap samples

Level $1 - \alpha$ for confidence interval

Output: A confidence interval for $P(Y = 1|C = c)$

init

Train classifier \mathcal{A} with training data $\{(Z'_i, Y'_i)\}_{i=1}^m$;

Calculate estimate $\hat{P}(Y = 1|C = c)$ with label shift methods (A.1) ;

Calculate label shift-corrected predictions $\mathcal{A}_L(Z_i, C_i)$ as in (2);

for $s = 1, \dots, B$ **do**

Sample $(Z_1^*, Y_1^*), \dots, (Z_m^*, Y_m^*)$ by resampling rows (Z'_i, Y'_i) with replacement;

Train classifier \mathcal{A}^* on bootstrap sample $(Z_1^*, Y_1^*), \dots, (Z_m^*, Y_m^*)$;

Sample (Z_i^*, C_i^*) by resampling rows (Z_i, C_i) with replacement;

Using (Z_i^*, Y_i^*) , \mathcal{A}^* , and Z_i^* , calculate $\hat{P}_s(Y^* = 1|C^* = c)$ with label shift methods (A.1);

end

return $1 - \alpha$ confidence interval from $\hat{P}(Y = 1|C = c)$ and the $\hat{P}_s(Y^* = 1|C^* = c)$ (e.g., a bootstrap percentile interval)

Algorithm 3: Semiparametric bootstrap confidence intervals with classifier predictions under label shift

Data: Labeled training data $\{(X'_i, Z'_i, Y'_i, C'_i, K'_i)\}_{i=1}^m$

Unlabeled test data $\{(X_j, Z_j, c_j, K_j)\}_{j=1}^n$

Input : Number B of bootstrap samples

Level $1 - \alpha$ for confidence interval

Output: A confidence interval for the parameters $\beta_{c,1}$ of the mixed effects model (5)

init

Train classifier \mathcal{A} with training data $\{(Z'_i, Y'_i)\}_{i=1}^m$;

Calculate label shift-corrected predictions $\mathcal{A}_L(Z_i, C_i)$ as in (2);

Fit the mixed effects model (5) for $y = 0$ and $y = 1$, using weights $w_{i,1} = \mathcal{A}_L(Z_i, c_i)$ and $w_{i,0} = 1 - w_{i,1}$.

This gives parameter estimates $\hat{\beta}_{c,y}$ and $\hat{\omega}^2$, and observed random effects \hat{b}_k ;

Define residuals $e_i = X_i - \hat{b}_k$;

for $s = 1, \dots, B$ **do**

Sample $(Z_1^*, Y_1^*), \dots, (Z_m^*, Y_m^*)$ by resampling rows (Z'_i, Y'_i) with replacement;

Train classifier \mathcal{A}^* on bootstrap sample $(Z_1^*, Y_1^*), \dots, (Z_m^*, Y_m^*)$;

Sample $(Z_i^*, C_i^*, K_i^*, \mathcal{A}_L(Z_i^*, c_i^*), e_i^*)$ by resampling rows $(Z_i, C_i, K_i, \mathcal{A}_L(Z_i, C_i), e_i)$ with replacement;

Sample $Y_i^* \stackrel{iid}{\sim} \text{Bernoulli}(\mathcal{A}_L(Z_i^*, C_i^*))$ for $i = 1, \dots, n$;

Sample $b_k^* \stackrel{iid}{\sim} N(0, \hat{\omega}^2)$ for $k \in \mathcal{K}$;

Generate X_i^* by $X_i^* = e_i^* + b_k^*$ for $i = 1, \dots, n$;

Using (Z_i^*, Y_i^*) , \mathcal{A}^* , and Z_i^* , calculate $\hat{P}(Y_i^* = 1|c_i^*)$ under the label shift assumption (A.1);

$$\mathcal{A}_L^*(Z_i^*, C_i^*) = \frac{\frac{\hat{P}(Y_i^* = 1|C_i^*)}{\hat{P}(Y_i^* = 1)} \mathcal{A}^*(Z_i^*)}{\frac{\hat{P}(Y_i^* = 1|C_i^*)}{\hat{P}(Y_i^* = 1)} \mathcal{A}^*(Z_i^*) + \frac{1 - \hat{P}(Y_i^* = 1|C_i^*)}{1 - \hat{P}(Y_i^* = 1)} (1 - \mathcal{A}^*(Z_i^*))};$$

Fit the mixed effects model (5) with observed data (X_i^*, C_i^*, K_i^*) and weights $w_{i,1}^* = \mathcal{A}_L^*(Z_i^*, C_i^*)$, giving estimates $\hat{\beta}_{c,1,s}$;

end

return $1 - \alpha$ confidence interval from $\hat{\beta}_{c,1}$ and the $\hat{\beta}_{c,1,s}^*$ (e.g., a bootstrap percentile interval)

Algorithm 4: Semiparametric bootstrap confidence intervals with mixture models under label shift

Data: Labeled training data $\{(X'_i, Z'_i, Y'_i, C'_i, K'_i)\}_{i=1}^m$
Unlabeled test data $\{(X_j, Z_j, C_j, K_j)\}_{j=1}^n$

Input : Number B of bootstrap samples
Level $1 - \alpha$ for confidence interval

Output: A confidence interval for the parameters $\beta_{c,1}$ of the mixture model (6)

init

Train classifier \mathcal{A} with training data $\{(Z'_i, Y'_i)\}_{i=1}^m$;
Using (Z'_i, Y'_i) , \mathcal{A} , and Z_i , calculate $\hat{P}(Y_i = 1|C_i)$ under the label shift assumption (A.1);
Calculate label shift-corrected predictions $\mathcal{A}_L(Z_i, C_i)$ as in (2);
Using $\hat{P}(Y_i = 1|C_i)$ as mixing proportions, fit the mixed effects mixture model (6), giving parameter estimates $\hat{\beta}_{c,y}$ and $\hat{\omega}_y^2$ and observed random effects $\hat{b}_{k,0}$, $y \in \{0, 1\}$;
Define residuals $e_{i,0} = X_i - \hat{b}_{k,1}$ and $e_{i,1} = X_i - \hat{b}_{k,0}$;

for $s = 1, \dots, B$ **do**

Sample $(Z_1^*, Y_1^*), \dots, (Z_m^*, Y_m^*)$ by resampling rows (Z'_i, Y'_i) with replacement;
Train classifier \mathcal{A}^* on bootstrap sample $(Z_1^*, Y_1^*), \dots, (Z_m^*, Y_m^*)$;
Sample $(Z_i^*, C_i^*, K_i^*, \mathcal{A}_L(Z_i^*, C_i^*), e_{i,0}^*, e_{i,1}^*)$ by resampling rows $(Z_i, C_i, K_i, \mathcal{A}_L(Z_i, C_i), e_{i,0}, e_{i,1})$ with replacement;
Sample $Y_i^* \stackrel{iid}{\sim} \text{Bernoulli}(\mathcal{A}_L(Z_i^*, c_i^*))$ for $i = 1, \dots, n$;
Sample $b_{k,0}^* \stackrel{iid}{\sim} N(0, \hat{\omega}_0^2)$ and $b_{k,1}^* \stackrel{iid}{\sim} N(0, \hat{\omega}_1^2)$ for $k \in \mathcal{K}$;
Generate X_i^* by $X_i^* = (e_{i,1}^* + b_{k,1}^*)Y_i^* + (e_{i,0}^* + b_{k,0}^*)(1 - Y_i^*)$ for $i = 1, \dots, n$;
Using (Z_i^*, Y_i^*) , \mathcal{A}^* , and Z_i^* , calculate $\hat{P}(Y_i^* = 1|C_i^*)$ under the label shift assumption (A.1);
Using $\hat{P}(Y_i^* = 1|C_i^*)$ as mixing proportions, fit the mixed effects mixture model (6), giving parameter estimates $\hat{\beta}_{c,1,s}^*$;

end

return $1 - \alpha$ confidence interval from $\hat{\beta}_{c,1}$ and the $\hat{\beta}_{c,1,s}^*$ (e.g., a bootstrap percentile interval)

(A3) holding true. We also assess the impact of deviations from parametric assumptions on the mixture model approach. In Table 5 we provide the simulation settings, describing how training and test data was simulated in each scenario. Note that $N(\mu, \sigma^2)$ denotes a Gaussian distribution with mean μ and variance σ^2 , and $SN(\xi, \omega, \alpha)$ denotes a skewed normal distribution with location ξ , scale ω , and shape α .

A.6 Functional PCA features

After automatic event detection and particle tracking, each detected event on the cell surface is represented by a series of grayscale 9×9 pixel frames, with the intensity of fluorescence recorded for each pixel. As shown in Figure 1, there are often clear differences in the individual frames for puffs and nonpuffs, and more importantly in the evolution of frames over time.

To capture the behavior of puffs over time, we first consider the two-dimensional intensity function within each frame. Noticing that puffs tend to have symmetric intensity functions, we can reduce the intensity function to a one-dimensional function of distance from the center of the frame (Figure 6). Each event then becomes a collection of radial intensity functions. As demonstrated in Figure 6, the radial intensity functions tend to have similar shapes, with only a few modes of variation. This suggests that functional PCA (fPCA) (Ramsay and Silverman, 2005) could provide effective dimension reduction of the radial profiles.

Before performing fPCA, each detected event was scaled to have the same peak intensity. Figure 6 shows the first two principal component functions, which together make up about 98% of the variability in radial intensity profiles. As we might expect, peak intensity in a frame is the main component of variation, captured by the first principal component. The second principal component, account for about 11% of the variability in radial intensity profiles, captures diffusivity of fluorescence in the frame. Each event is then represented as

Algorithm 5: Semiparametric bootstrap confidence intervals with classifier predictions under label shift, with variance calibration step

Data: Labeled training data $\{(X'_i, Z'_i, Y'_i, C'_i, K'_i)\}_{i=1}^m$
 Unlabeled test data $\{(X_j, Z_j, c_j, K_j)\}_{j=1}^n$

Input : Number B of bootstrap samples
 Level $1 - \alpha$ for confidence interval

Output: A confidence interval for the parameters $\beta_{c,1}$ of the mixed effects model (5)

init

Train classifier \mathcal{A} with training data $\{(Z'_i, Y'_i)\}_{i=1}^m$;
 Calculate label shift-corrected predictions $\mathcal{A}_L(Z_i, C_i)$ as in (2);
 Fit the mixed effects model (5) with $y = 1$ and weights $w_{i,1} = \mathcal{A}_L(Z_i, c_i)$, giving parameter estimates $\hat{\beta}_{c,1}$ and $\hat{\omega}_1^2$, and observed random effects $\hat{b}_{k,1}$;
 Fit the mixed effects model (5) with $y = 0$ and weights $w_{i,0} = 1 - w_{i,1}$, giving parameter estimates $\hat{\beta}_{c,0}$ and $\hat{\omega}_0^2$, and observed random effects $\hat{b}_{k,0}$;
 Define residuals $e_{i,0} = X_i - \hat{b}_{k,1}$ and $e_{i,1} = X_i - \hat{b}_{k,0}$;

for $s = 1, \dots, B$ **do**

Sample $(Z_1^*, Y_1^*), \dots, (Z_m^*, Y_m^*)$ by resampling rows (Z'_i, Y'_i) with replacement;
 Train classifier \mathcal{A}^* on bootstrap sample $(Z_1^*, Y_1^*), \dots, (Z_m^*, Y_m^*)$;
 Sample $(Z_i^*, C_i^*, K_i^*, \mathcal{A}_L(Z_i^*, C_i^*), e_{i,0}^*, e_{i,1}^*)$ by resampling rows $(Z_i, C_i, K_i, \mathcal{A}_L(Z_i, C_i), e_{i,0}, e_{i,1})$ with replacement;
 Sample $Y_i^* \stackrel{iid}{\sim} \text{Bernoulli}(\mathcal{A}_L(Z_i^*, C_i^*))$ for $i = 1, \dots, n$;
 Sample $b_{k,0}^* \stackrel{iid}{\sim} N(0, \hat{\omega}_0^2)$ and $b_{k,1}^* \stackrel{iid}{\sim} N(0, \hat{\omega}_1^2)$ for $k \in \mathcal{K}$;
 Generate X_i^* by $X_i^* = (e_{i,1}^* + b_{k,1}^*)Y_i^* + (e_{i,0}^* + b_{k,0}^*)(1 - Y_i^*)$ for $i = 1, \dots, n$;
 Using (Z_i^*, Y_i^*) , \mathcal{A}^* , and Z_i^* , calculate $\hat{P}(Y_i^* = 1 | c_i^*)$ under the label shift assumption (A.1);

$$\mathcal{A}_L^*(Z_i^*, C_i^*) = \frac{\frac{\hat{P}(Y_i^* = 1 | C_i^*)}{\hat{P}(Y_i^* = 1)} \mathcal{A}^*(Z_i^*)}{\frac{\hat{P}(Y_i^* = 1 | C_i^*)}{\hat{P}(Y_i^* = 1)} \mathcal{A}^*(Z_i^*) + \frac{1 - \hat{P}(Y_i^* = 1 | C_i^*)}{1 - \hat{P}(Y_i^* = 1)} (1 - \mathcal{A}^*(Z_i^*))};$$

Fit the mixed effects model (5) with observed data (X_i^*, C_i^*, K_i^*) and weights $w_{i,1}^* = \mathcal{A}_L^*(Z_i^*, C_i^*)$ and $w_{i,0}^* = 1 - w_{i,1}^*$, giving estimates $\hat{\omega}_{1,s}^{*2}$ and $\hat{\omega}_{0,s}^{*2}$;
 Calculate the true sample variance $v_{y,s}^2 = \frac{1}{|\mathcal{K}| - 1} \sum_k b_{k,y}^{*2}$;

end

Regress $v_{y,s}^2$ on $\hat{\omega}_{y,s}^{*2}$, producing an estimating function \hat{f}_y with $\hat{v}_{y,s}^2 = \hat{f}_y(\hat{\omega}_{y,s}^{*2})$, for $y \in \{0, 1\}$;

Calculate the adjusted variances: $\hat{\omega}_{y,\text{adj}}^2 = \hat{f}_y(\hat{\omega}_y^{*2})$, for $y \in \{0, 1\}$;

for $s = 1, \dots, B$ **do**

Sample $(Z_1^*, Y_1^*), \dots, (Z_m^*, Y_m^*)$ by resampling rows (Z'_i, Y'_i) with replacement;
 Train classifier \mathcal{A}^* on bootstrap sample $(Z_1^*, Y_1^*), \dots, (Z_m^*, Y_m^*)$;
 Sample $(Z_i^*, C_i^*, K_i^*, \mathcal{A}_L(Z_i^*, C_i^*), e_{i,0}^*, e_{i,1}^*)$ by resampling rows $(Z_i, C_i, K_i, \mathcal{A}_L(Z_i, C_i), e_{i,0}, e_{i,1})$ with replacement;
 Sample $Y_i^* \stackrel{iid}{\sim} \text{Bernoulli}(\mathcal{A}_L(Z_i^*, C_i^*))$ for $i = 1, \dots, n$;
 Sample $b_{k,0}^* \stackrel{iid}{\sim} N(0, \hat{\omega}_{0,\text{adj}}^2)$ and $b_{k,1}^* \stackrel{iid}{\sim} N(0, \hat{\omega}_{1,\text{adj}}^2)$ for $k \in \mathcal{K}$;
 Generate X_i^* by $X_i^* = (e_{i,1}^* + b_{k,1}^*)Y_i^* + (e_{i,0}^* + b_{k,0}^*)(1 - Y_i^*)$ for $i = 1, \dots, n$;
 Using (Z_i^*, Y_i^*) , \mathcal{A}^* , and Z_i^* , calculate $\hat{P}(Y_i^* = 1 | c_i^*)$ under the label shift assumption (A.1);

$$\mathcal{A}_L^*(Z_i^*, C_i^*) = \frac{\frac{\hat{P}(Y_i^* = 1 | C_i^*)}{\hat{P}(Y_i^* = 1)} \mathcal{A}^*(Z_i^*)}{\frac{\hat{P}(Y_i^* = 1 | C_i^*)}{\hat{P}(Y_i^* = 1)} \mathcal{A}^*(Z_i^*) + \frac{1 - \hat{P}(Y_i^* = 1 | C_i^*)}{1 - \hat{P}(Y_i^* = 1)} (1 - \mathcal{A}^*(Z_i^*))};$$

Fit the mixed effects model (5) with observed data (X_i^*, C_i^*, K_i^*) and weights $w_{i,1}^* = \mathcal{A}_L^*(Z_i^*, C_i^*)$, giving estimates $\hat{\beta}_{c,1,s}^*$;

end

return $1 - \alpha$ confidence interval from $\hat{\beta}_{c,1}$ and the $\hat{\beta}_{c,1,s}^*$ (e.g., a bootstrap percentile interval)

Assumptions	Normal?	Training Data	Test Data
(A1), (A2), (A3)	yes	$Y' \sim \text{Bernoulli}(0.2)$ $Z' Y' = 0 \sim N(0, 1)$ $Z' Y' = 1 \sim N(3, 1)$	$Y \sim \text{Bernoulli}(0.4)$ $Z Y = 0 \sim N(0, 1)$ $Z Y = 1 \sim N(3, 1)$ $b_k \sim N(0, 0.5)$ $X_i = Z_i + b_{k_i} + N(0, 0.2)$
	no	$Y' \sim \text{Bernoulli}(0.2)$ $Z' Y' = 0 \sim SN(0, 2, 3)$ $Z' Y' = 1 \sim 8 - SN(3, 2, 3)$	$Y \sim \text{Bernoulli}(0.4)$ $Z Y = 0 \sim SN(0, 2, 3)$ $Z Y = 1 \sim 8 - SN(3, 2, 3)$ $b_k \sim N(0, 0.5)$ $X_i = Z_i + b_{k_i} + N(0, 0.2)$
(A2), (A3)	yes	$Y' \sim \text{Bernoulli}(0.2)$ $Z' Y' = 0 \sim N(-0.5, 1)$ $Z' Y' = 1 \sim N(3, 1)$	$Y \sim \text{Bernoulli}(0.4)$ $Z Y = 0 \sim N(0, 1)$ $Z Y = 1 \sim N(3, 1)$ $b_k \sim N(0, 0.5)$ $X_i = Z_i + b_{k_i} + N(0, 0.2)$
	no	$Y' \sim \text{Bernoulli}(0.2)$ $Z' Y' = 0 \sim SN(-0.5, 2, 3)$ $Z' Y' = 1 \sim 8 - SN(3, 2, 3)$	$Y \sim \text{Bernoulli}(0.4)$ $Z Y = 0 \sim SN(0, 2, 3)$ $Z Y = 1 \sim 8 - SN(3, 2, 3)$ $b_k \sim N(0, 0.5)$ $X_i = Z_i + b_{k_i} + N(0, 0.2)$
(A1), (A2)	yes	$Y' \sim \text{Bernoulli}(0.2)$ $Z' Y' = 0 \sim N(0, 1)$ $Z' Y' = 1 \sim N(3, 1)$	$Y \sim \text{Bernoulli}(0.4)$ $Z Y = 0 \sim N(0, 1)$ $Z Y = 1 \sim N(3, 1)$ $b_k \sim N(0, 0.5)$ $X_i = Z_i + b_{k_i} + N(0, 0.2) + \mathbb{1}(Y_i = 1)$
	no	$Y' \sim \text{Bernoulli}(0.2)$ $Z' Y' = 0 \sim SN(0, 2, 3)$ $Z' Y' = 1 \sim 8 - SN(3, 2, 3)$	$Y \sim \text{Bernoulli}(0.4)$ $Z Y = 0 \sim SN(0, 2, 3)$ $Z Y = 1 \sim 8 - SN(3, 2, 3)$ $b_k \sim N(0, 0.5)$ $X_i = Z_i + b_{k_i} + N(0, 0.2) + \mathbb{1}(Y_i = 1)$

Table 5: Simulation settings for assessing performance of bootstrap inference procedures.

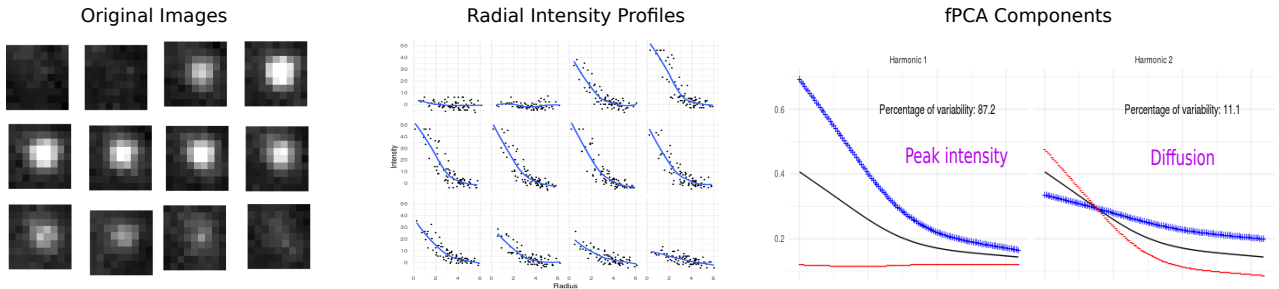


Figure 6: Functional PCA on radial intensity profiles. Left: the original frames for a puff from TIRF microscopy. Center: the corresponding radial intensity profiles for the frames on the left, with smooth curves showing the overall shape in each frame. Right: the first two fPCA component functions for the radial intensity profiles, plotted as differences from the mean function (the black curve). A positive score for the component function is plotted with blue +’s, while a negative score for the component function is plotted with red –’s.

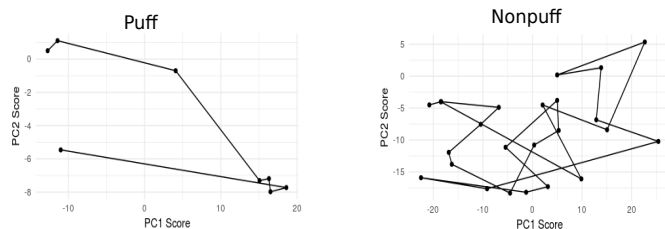


Figure 7: Differences between fPCA score paths for puffs and nonpuffs.

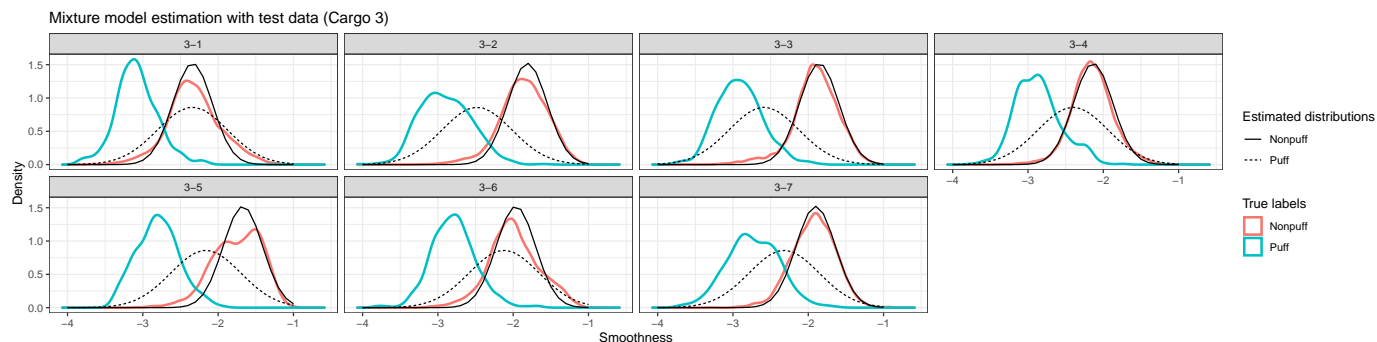


Figure 8: The distribution of *Smoothness* in each cell, for puffs and nonpuffs. Estimates of the true densities are shown from kernel density estimation with the true labels, while the black curves show the fitted normal distributions from a hierarchical Gaussian mixture model. For the mixture model, the mixing proportion for puffs and nonpuffs is estimated as a parameter of the model.

a bivariate time series of scores for the first two principal components. As suggested by Figure 1, time series of component scores for puffs are expected to have a characteristic pattern, whereas scores for nonpuffs are expected to be much noisier. To visualize fPCA score time series, we consider each event as a path through two-dimensional principal component score space. Figure 7 shows these paths for a puff and a nonpuff, illustrating the differences we expect to see in these time series.

Figure 7 suggests that featurizing the fPCA score paths could be useful for classifying puffs and nonpuffs. We construct several features:

- *ConvexArea* and *ConvexPerimeter*: the area and perimeter of a convex hull around the score path
- *Noise*: a measure of randomness in the time series of first principal component scores
- *Smoothness*: the average distance between points in the observed score path and the kernel-smoothed score path

A.7 TIRF microscopy mixture model results

In Section 5, we summarize the results of inference on puff *Smoothness*, using the mixed effects approach and the mixture model approach. The full results are provided here. Figure 8 shows the distribution of *Smoothness* within each test cell, for puffs and nonpuffs. The distributions in Figure 8 suggest that a two-component Gaussian mixture is reasonable, and so we fit the hierarchical mixture described in (6). However, because the parametric model does not hold exactly, and the proportion of puffs is small, the estimated puff distributions are poor (Figure 8). With the mixing proportions specified, Figure 9 shows the resulting fit, which is much improved over Figure 8. The estimated means in each cell are given by Table 6; the slight bias in puff means arises because the distribution of *Smoothness* is only approximately Gaussian.

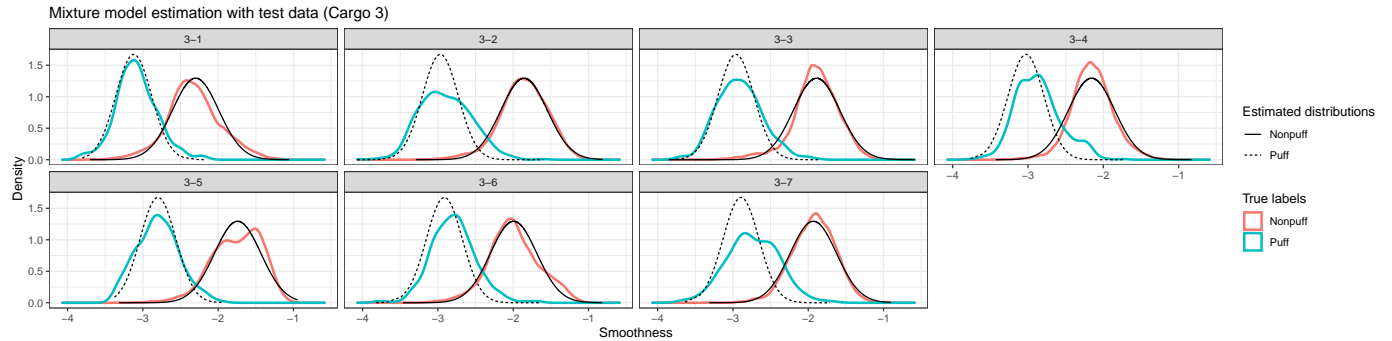


Figure 9: The distribution of *Smoothness* in each cell, for puffs and nonpuffs. Estimates of the true densities are shown from kernel density estimation with the true labels, while the black curves show the fitted normal distributions from a hierarchical Gaussian mixture model. For the mixture model, the mixing proportion in each cell is estimated beforehand with the label shift correction, to improve identifiability.

Cell	True means		Mixture model estimates	
	Puff	Nonpuff	Puff	Nonpuff
3-1	-3.08	-2.32	-3.12	-2.30
3-2	-2.90	-1.86	-2.97	-1.86
3-3	-2.91	-1.90	-2.96	-1.89
3-4	-2.87	-2.15	-3.03	-2.16
3-5	-2.80	-1.75	-2.80	-1.74
3-6	-2.79	-1.99	-2.91	-1.99
3-7	-2.73	-1.93	-2.89	-1.93

Table 6: Mean of *Smoothness* in each Condition 3 cell. The true means are estimated with the true labels, while the mixture model estimates result from a mixed effects Gaussian mixture model (6), where the mixing proportion in each cell is estimated with the label shift correction. There is slight bias in the mixture model estimates of puff means shown here; this occurs because the distribution of *Smoothness* for puffs is only approximately Gaussian, and is slightly right-skewed (Figure 9).